North Reduced Fluid Simulation - Prelimenary Results

Rune Højlund

December 22, 2022

This is a note presenting the prelimenary results from reduced fluid simulations conducted at the department of Physics, DTU in 2022. The project was originally done by Asbjørn C. Pedersen and myself, Rune Højlund together with Alexander Simon Thrysøe, Anders Henry Nielsen and Aslak Sindbjerg Poulsen as supervisors. In June 2022 Asbjørn and I handed in a project report [13]. The following sections reuse in full or some part content from the original project report [13]: Section 1.1, 2, 3.2.3, 3.3.3, 3.3.4, 4, G.

Contents

1 Introduction

In order to enhance the energy confinement time of magnetically confined plasmas it is important to understand the turbolent transport of particles and heat. For this purpose we have implemented a reduced fluid model describing the dynamics of the NORTH tokamak located at DTU, Lyngby.

1.1 Toroidal Geometry of NORTH

The transport experiments which we simulate in this work were carried out without the central solenoid. Thus, we assume there were no toroidal plasma current and the magnetic confinement is therefore not a tokamak-geometry, but rather a simple magnetised torus. This toroidal geometry can be described by the curvilinear coordinates $(u^1, u^2, u^3) = (r, \zeta, \theta)$, where $u^1 = r$ is the minor radius, $u^2 = \zeta$ is the toroidal angle (in the direction of the $\mathbf{B}$-field) and $u^3 = \theta$ is the poloidal angle as illustrated on Figure 1.

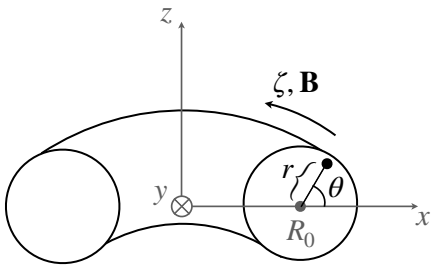

Figure 1: Illustration of toroidal curvilinear coordinates.

In this geometry, the magnetic field is given by:

$$\mathbf{B} = \frac{B_0 R_0}{R} \hat{\boldsymbol{\zeta}}. \tag{1}$$

With the parameters of NORTH and using Ampere's law, the magnetic field at the major radius R_0 is calculated to be $B_0 = 0.077\,\mathrm{T}$. This is the magnetic field strength which we use in the model.

2 The ESEL Model

We use the ESEL model as our reduced fluid model for simulating the dynamics of the NORTH tokamak perpendicular to the magnetic field. A partial derivation is seen in Section 7 and more details are found in [7, 8]. The following references are also helpful in deriving the ESEL equations: [12, 14, 3, 9]. The equations describe the evolution of the electron density, n, vorticity, Ω, and temperature, T:

$$\begin{aligned}
\frac{\mathrm{d}n'}{\mathrm{d}t'} + n'\mathcal{C}'(\phi') - \mathcal{C}'(n'T_e') &= \Lambda_n' \\
\frac{\mathrm{d}\Omega'}{\mathrm{d}t'} - \mathcal{C}'(n'T_e') &= \Lambda_\Omega' \\
\frac{\mathrm{d}T_e'}{\mathrm{d}t'} + \frac{2T_e'}{3}\mathcal{C}'(\phi') - \frac{7T_e'}{3}\mathcal{C}'(T_e') - \frac{2T_e'^2}{3n'}\mathcal{C}'(n') &= \Lambda_{T_e}'
\end{aligned}$$

where the right hand side of each equation contains diffusion and external sources S' and sinks L'

$$\Lambda_n' = D_{n'}'\nabla_\perp^2 n' + S_{n'}'(r', \theta') - L_{n'}'(r', \theta') \tag{2}$$

$$\Lambda_{T_e}' = D_{T_e'}'\nabla_\perp^2 T_e' + S_{T_e'}'(r', \theta') - L_{T_e'}'(r', \theta') \tag{3}$$

$$\Lambda_\Omega' = D_{\Omega'}'\nabla_\perp^2 \Omega' - L_{\Omega'}'(r', \theta') \tag{4}$$

All the primed equations and fields are non-dimensionalized according to

$$\begin{aligned} x' &= \frac{\mathbf{x}}{\rho_{\mathrm{s},0}} \quad t' = t\omega_{\mathrm{ci},0} \quad B' = \frac{B}{B_0} \\ n' &= \frac{n}{n_0} \quad T'_{\mathrm{e}} = \frac{T_{\mathrm{e}}}{T_{\mathrm{e}0}} \quad \phi' = \frac{e\phi}{T_{\mathrm{e},0}}, \end{aligned} \tag{5}$$

where $B_0 = 0.077\mathrm{T}$, corresponding to the magnetic field in the centre of NORTH, $\omega_{ci,0} = qB_0/m_i$ is the characteristic ion cyclotron frequency, $\rho_{s,0} = c_{s,0}/\omega_{ci,0}$ is the characteristic ion Larmor radius and

$$c_{s,0} = (T_{e,0}/m_i)^{1/2} \tag{6}$$

is the cold ion acoustic speed. $\mathcal{C}'$ is the non-dimensionalized curvature operator which in our geometry is (see Section D):

$$\mathcal{C}' = \frac{\rho_{s,0}}{R_0}\frac{\partial}{\partial z'}. \tag{7}$$

3 Physical Assumptions

As input for the model we used the following parameters:

3.1 Diffusion Coefficients

We tried using diffusion coefficients calculated from first principles. Therefore all diffusion coefficients for both density, temperature and vorticity were set to 5×10^{-3}.

3.2 Sources

3.2.1 Density

We assume new particles are created by electron impact ionisation. The density source is calculated from the ionization rate which is determined by the cross section of electron impact collisions [15]:

$$S_n = (\partial_t n)^{\mathrm{iz}} = n_n n \langle \sigma_{\mathrm{iz}} v \rangle = n_n n k_{\mathrm{iz}}, \tag{8}$$

$$k_{\mathrm{iz}} = 2 \cdot 10^{-13} \frac{\sqrt{T_{\mathrm{e}}/(-E_{ion})}}{6 + T_{\mathrm{e}}/(-E_{ion})} \exp\left(-\frac{-E_{ion}}{T_{\mathrm{e}}}\right) \quad \mathrm{m^3 s^{-1}}. \tag{9}$$

3.2.2 Vorticity

We have no source for the vorticity.

3.2.3 Temperature

Since the model doesn't consider parallel transport and covers the entire poloidal cross section of the vacuum vessel, the only source of electron temperature is an external heating source. This introduces the source term

$$S'_{Te}(r,\theta) = \frac{\Delta T'_{e,S} p(r,\theta)}{\tau'_S}, \tag{10}$$

where $p(r,\theta)$ is the profile of the heating source. To mimic the ECR hearing from the LFS launcher, the profile of the heating source is a narrow Gaussian around the ECR. In Toroidal coordinates, the profile in the poloidal plane is

$$p(r,\theta) = \frac{1}{2\pi\sigma_R\sigma_z} \exp\left[-\frac{(R_0 + r\cos\theta - R_{res})^2}{2\sigma_R^2} - \frac{(r\sin\theta)^2}{2\sigma_z^2} \right], \tag{11}$$

where R_{res} is the radial distance of the ECR from the symmetry axis and σ_R^2 and σ_z^2 are the variances of the profile in the axial direction and radial direction from the symmetry axis respectively,

here set to $\sigma_R = 0.005$m and $\sigma_z = 0.03$m. The position of the electron cyclotron resonance in NORTH with the chosen toroidal current of 1000A is $R_{res} = 0.219$m. Fig. 2 shows a contour plot of the heating source profile. All of the external power from the heating source P_S is deposited as an increase in temperature. Therefore,

$$P_S = \int \mathrm{d}V \frac{3}{2} \left(\frac{\partial p}{\partial t} \right)_S = \frac{3}{2} \int \mathrm{d}V n \left(\frac{\partial T_e}{\partial t} \right)_S , \tag{12}$$

where the index S refers to changes due to the external source. The volume intregral is calculated with the Jacobian from (51) in the Appendix. Numerically, the derivative in Eq. (12) is calculated by

$$\left(\frac{\partial T_e(r,\theta)}{\partial t} \right)_S = \frac{\Delta T p(r,\theta)}{\tau_S}, \tag{13}$$

where τ_S is a characteristic time scale for the source. Then

$$\frac{\Delta T(r,\theta)}{\tau_S} = \frac{2P_S}{3\int \mathrm{d}V n(r,\theta) p(r,\theta)} \approx \frac{2P_S}{3\int \mathrm{d}V p(r,\theta)} \frac{1}{n(r,\theta)}. \tag{14}$$

In the last step, the integral is approximated by a kind of local density approximation (LDA) in order to effectively evaluate the integral and decrease the computation time significantly. Thus, if the local density is large we heat less which seems to make physical sense.

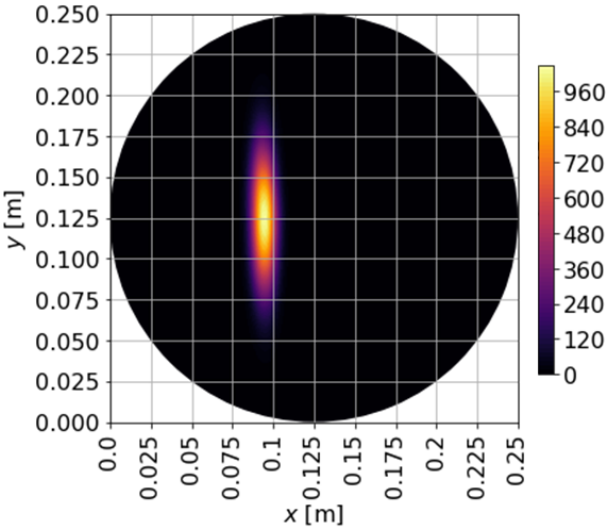

Figure 2: Contour plot of the profile $p(r,\theta)$.

3.3 Sinks

3.3.1 Density

Similar to the density source, Eq. (8), we calculate the density loss from radiative recombination from the cross section:

$$L_n = -(\partial_t n)^{\mathrm{rc}} = n\, n\, \langle \sigma_{\mathrm{rc}} v_e \rangle = n^2\, k_{\mathrm{rc}}.$$

The recombination rate k_{rc} can be found in [14].

3.3.2 Vorticity

Recombination might also create a sink in the vorticity. This is not currently treated in a systematic manner. Instead, also mostly to obtain stability, we currently have just implemented an artificial

global sink in the vorticity:

$$L_\Omega = \frac{\Omega}{\tau} \tag{15}$$

3.3.3 Temperature

When neutral particles are ionized, the energy is delivered through collisions with electrons. The energy required to ionize a neutral particle and increase the temperature of the new electron to that of the surrounding electrons T_e, requires an energy of $-E_{ion} + T_e$. Therefore the ionization process leads to a corresponding (Bohm normalized) temperature sink of

$$L'_{T_e}(r,\theta) = -(-E'_{ion} + T'_e)\frac{S'_n(r,\theta)}{n'_e(r,\theta)}. \tag{16}$$

3.3.4 Wall Interactions

When plasma particles reach the conducting wall of the vacuum vessel there is a loss of both particles, temperature and momentum. Due to the finite Larmor radius of the particle orbits, the losses are expected to happen within one ion Larmor radius of the wall. Thus, all loss terms are linear

$$L_n(r,\theta) = -\frac{n(r,\theta)\sigma_w(r,\theta)}{\tau_{w,n}} \tag{17}$$

$$L_{T_e}(r,\theta) = -\frac{T_e(r,\theta)\sigma_w(r,\theta)}{\tau_{w,T_e}} \tag{18}$$

$$L_\Omega(r,\theta) = -\frac{\Omega(r,\theta)\sigma_w(r,\theta)}{\tau_{w,\Omega}}, \tag{19}$$

where $\tau_{w,n}$, τ_{w,T_e} and $\tau_{w,\Omega}$ are the loss times of particles, electron temperature and vorticity and the wall loss profile $\sigma_w(r,\theta)$ is

$$\sigma_w(r,\theta) = \frac{1}{2} + \frac{1}{2}\tanh\frac{r - (R_0/2 - \rho_{s,0})}{0.001} \tag{20}$$

and is plotted in Fig. 3. Typical radial speed of plasma particles at the outer edge is a fraction of the cold ion sound speed, while the typical parallel speed is substantially larger. The particle loss time is set to the time it takes a particle moving with a speed of $0.1c_{s,0}$ to move the distance of a cold ion Larmor radius

$$\tau'_{w,n} = \frac{\rho_{s,0}\omega_{ci,0}}{0.1c_{s,0}} \approx 14.1. \tag{21}$$

The loss time for vorticity is set equally $\tau'_\Omega = \tau'_{w,n}$. Due to the tendency for hot electrons to be lost faster than colder electrons as noted in [7], loss time for electron temperature is set twice as low as the density loss time $\tau'_{T_e} = 0.5\tau'_{w,n} \approx 7.1$.

3.4 Boundary conditions

Since we only simulate the poloidal 2D-domain, we only need to consider the boundaries in the r and θ direction. For θ we of course have periodic boundaries for all fields f, such that $f\Big|_{\theta=0} = f\Big|_{\theta=2\pi}$. Meanwhile, in the radial direction at $r = a$ we apply Neumann-conditions for all fields:

$$\left.\frac{\partial n}{\partial r}\right|_{r=a} = 0 \quad \text{(density)} \tag{22a}$$

$$\left.\frac{\partial T_e}{\partial r}\right|_{r=a} = 0 \quad \text{(electron temperature)} \tag{22b}$$

$$\left.\frac{\partial \Omega}{\partial r}\right|_{r=a} = 0 \quad \text{(vorticity)} \tag{22c}$$

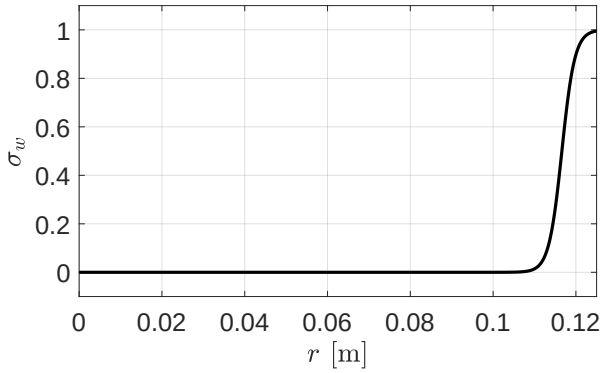

Figure 3: Profile of the wall sink.

There is no real physical justification for this choice. The temperature and vorticity are unconstrained at the boundary, and the density should vanish at the wall, but we have already attempted to account for the wall absorption of particles, energy and momentum through the sinks in Section 3.3.4. Finally, the BC at $r = 0$ is dealt with in Section G.5.

4 Implementation

The model is implemented in the C++ framework, BOUT++, which was jointly developed by University of York, LLNL, CCFE, DCU, DTU, and other international partners [5, 6]. Bout++ was specifically developed with fluid plasma simulations in curvilinear coordinates in mind. All code for our implementation and data analysis is available on GitHub [1]. More details on the implementation can be found in Section G.

5 Results

Plots of the results can be found in the GitHub Repository at https://github.com/PPFE-Turbulence/north-simulation/tree/master/presentation of main results. At the link the reader will also find animations of the density, vorticity, temperature, pressure, electric field and density source which we due to the physical constraints of this document naturally cannot present here.

On Figure 4 we see a time series of the transient behaviour before the plasma reaches steady state. We see a pertubation in the plasma density (blob) arising close to the center due to electron impact ionization from the ECR heating. The blob then propagates outwards in a mushroom shape. At about 500 μs the plasma begins to form two centers below and above in the domain. It turns out that these two centers rotate in opposite directions in a steady-state configuration. The initial transient behavior can be explained by the interchange mechanism (see [13, 8]).

The total simulated time in the results presented is about 3000 μs and after about 1500 μs the system has clearly settled on a surprising steady state configuration which can be inspected by considering the time-average fields of the last 1500 μs. This is shown in Figure 5. On the figure we see that the steady state configuration has two centers in the density, Figure 5a with opposite signs of the charge buildup (as seen on Figure 5e) and therefore opposite vorticities, Figure 5b. By model design, the temperature on Figure 5c heats around the electron cyclotron frequency and new particles are created on Figure 5d as the plasma is heated. In the pressure profile on Figure 5f. On Figure 6 we see the evolution of the mean field values (spatially averaged). As such on Figure 6a we see the total charge buildup in the plasma. On Figure 6b is shown the mean temperature in the domain and on Figure 6c we show the contained energy calculated as the volume integral of the pressure. For all three quantities we note that a transient is followed by a flattening steady-state value. A simple estimate of the energy confinement time of NORTH is obtained by dividing the

contained energy with the supplied power:

$$\tau_E = \frac{E}{P_{\text{ext}}} \approx 0.8\,\text{ms}.$$

To simulate the Langmuir probes of the experimental setup of NORTH we have included 12 fast-output points in the simulation. The simulation probes were evenly spaced at the $\theta = 0$ axis with positions from $r = 0\,\text{cm}$ to $r = a = 12.5\,\text{cm}$. These probes spit out higher temporal-resolution simulation data. Density readings from 5 of the probes are shown in Figure 7. On the probe measurements we again see the transient followed by a steady state fluctuation. The last probe is closed to the wall where our wall-sink kills any signal. The transient probe measurements are shown in Figure 8 where we see a radial delay in the probe signal which reflects the outwards propagating blob. Meanwhile on Figure 9 we see the steady state signals which all have a sawtooth-like pattern with a well-defined period.

As our final analysis, we present on Figure 10 the density signal of the probe at $r = a/2 = 6.25\,\text{cm}$ in the steady state. We have calculated the fast fourier transform of the signal and obtain a well-defined frequency at $10.0\,\text{kHz}$ with a visible second and third harmonic. One might speculate that this characteristic frequency can be tuned by changing the experimental parameters such as the power. This might be a good way to verify the simulation results. A sinusoidal fit with the given frequency shows that the amplitude is about 12% of the signal mean value.

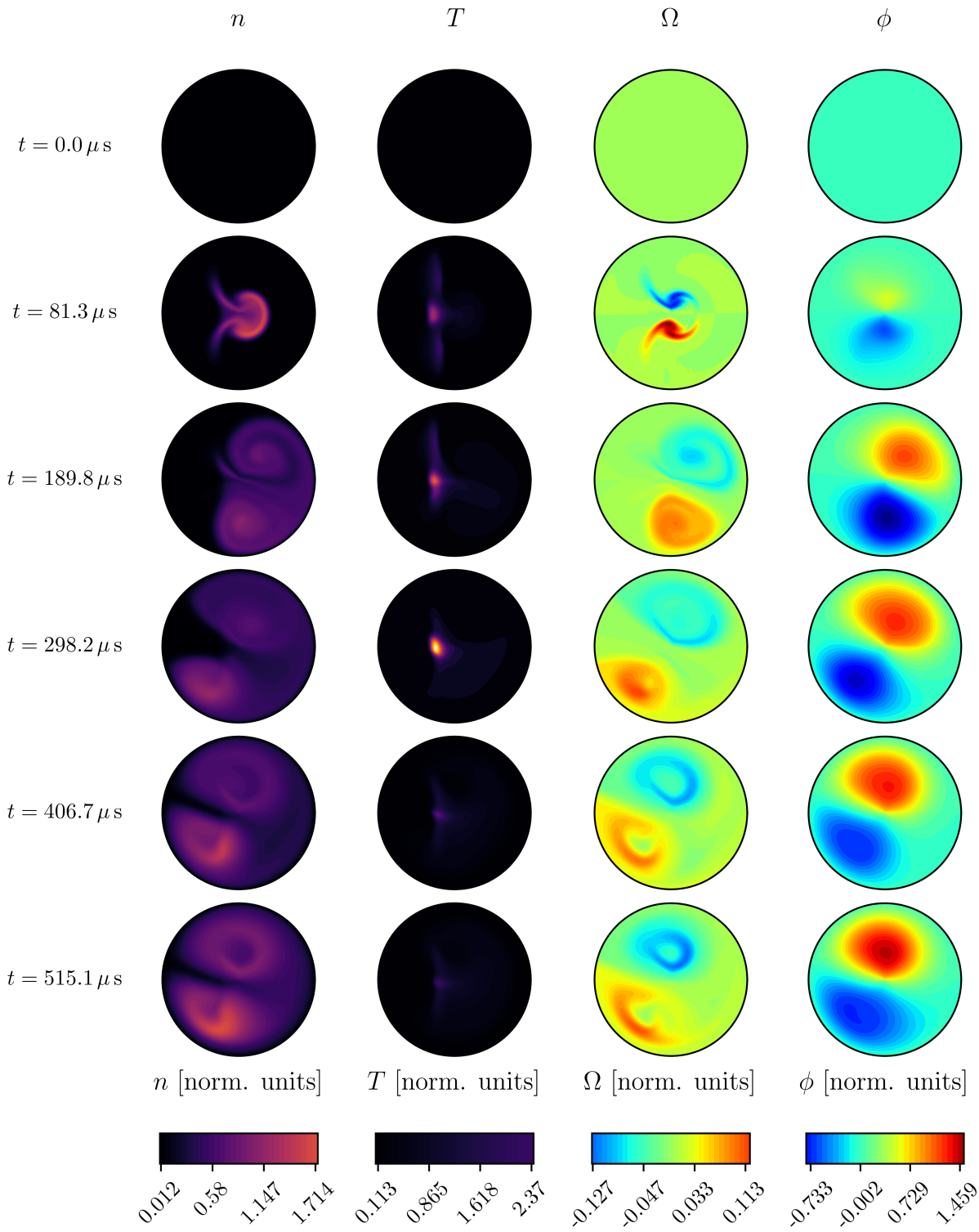

Figure 4: Poloidal plane contour plots of simulation results for the density, n, temperature, T, vorticity, Ω and electric potential ϕ to illustrate the temporal development. All scales are in normalised units.

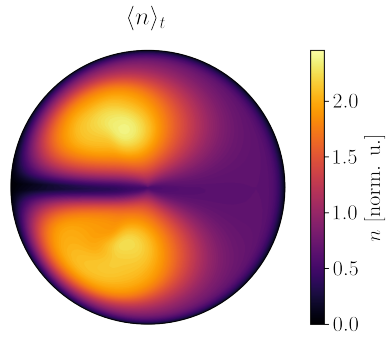

(a) Density

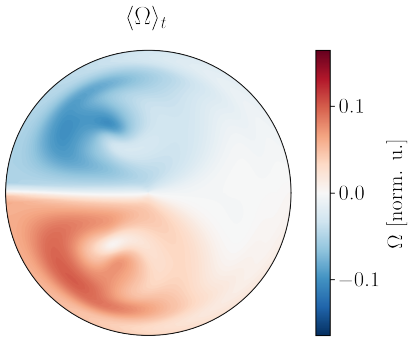

(b) Vorticity

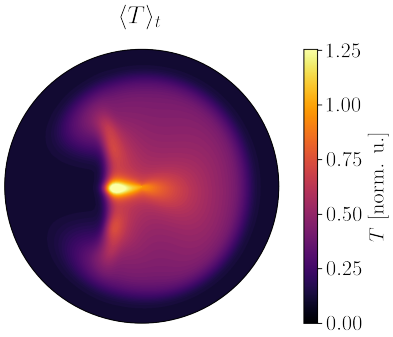

(c) Temperature

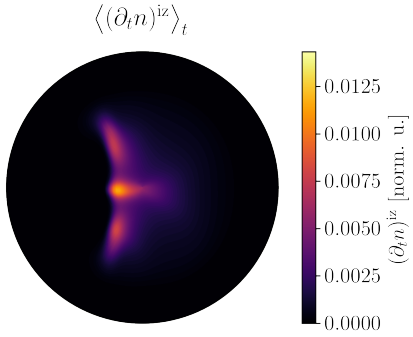

(d) Density source from electron impact ionization

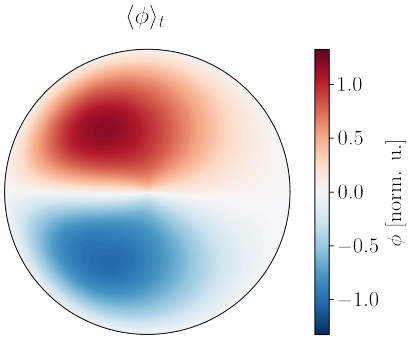

(e) Electric field

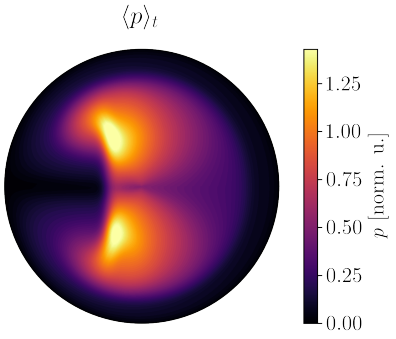

(f) Pressure

Figure 5: Poloidal profiles of fields which have been averaged over time in the steady state period of the simulation.

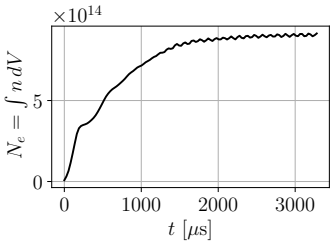

(a) Total number of charges

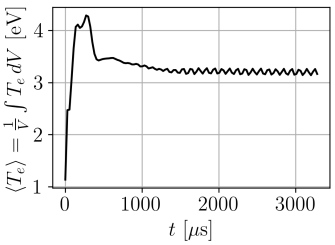

(b) Mean Temperature

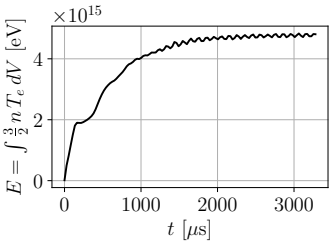

(c) Contained Energy

Figure 6: Evolution of spatially averaged fields as a function of time.

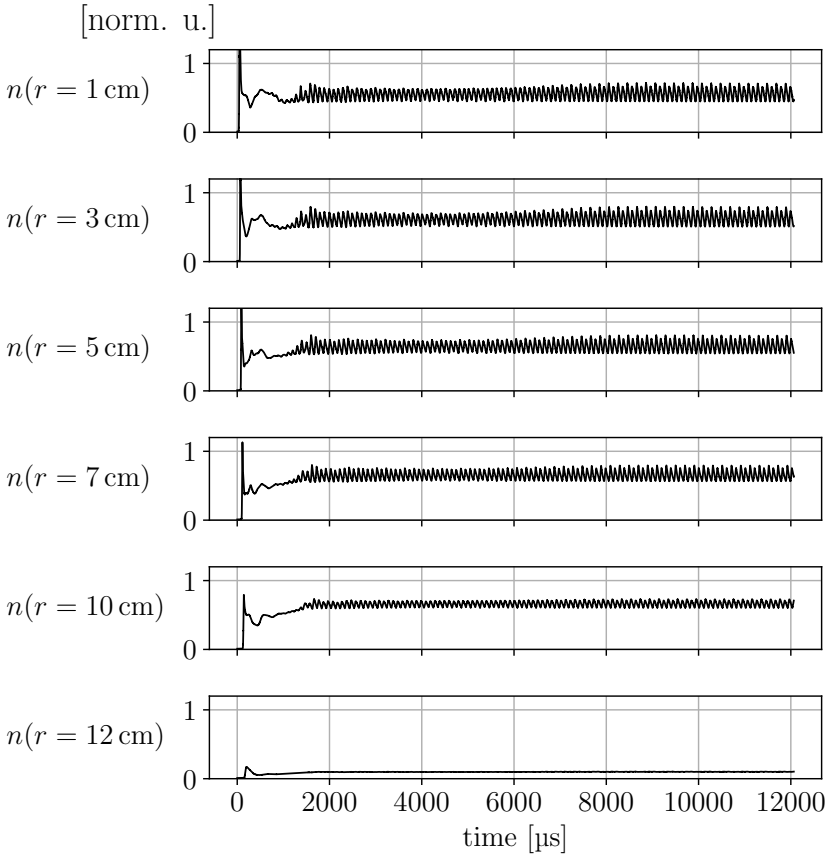

Figure 7: Density reading from 5 fast probes

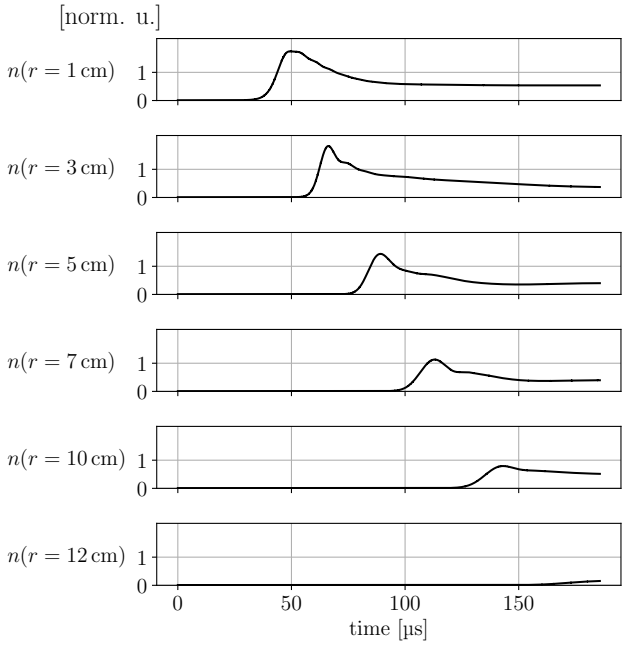

Figure 8: Density reading from 5 fast probes (transient)

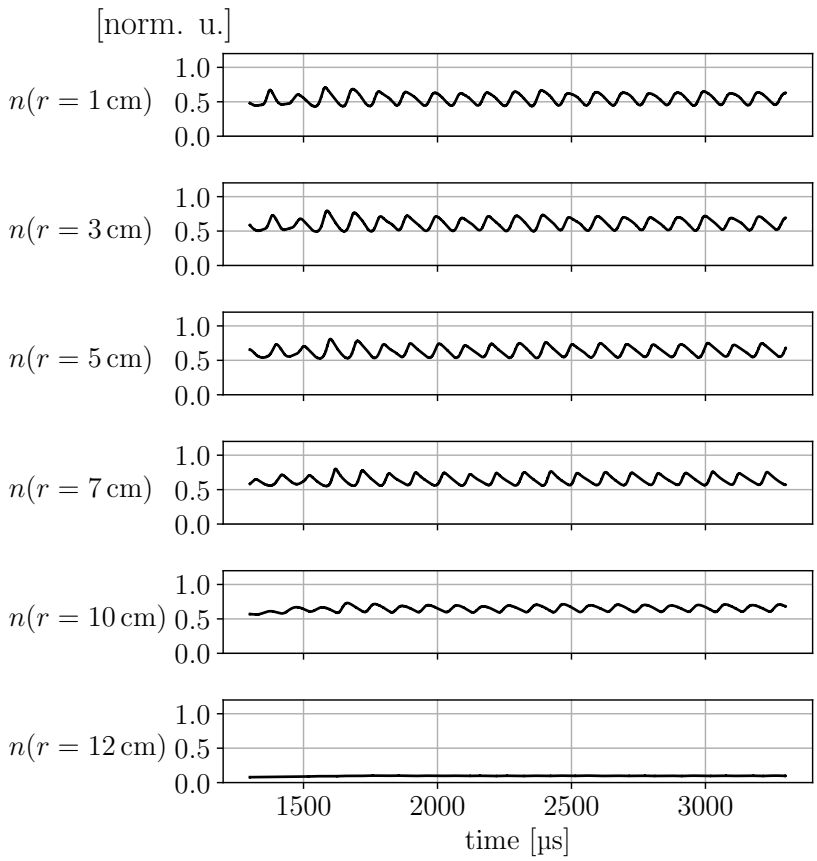

Figure 9: Density reading from 5 fast probes (steady state)

(a)

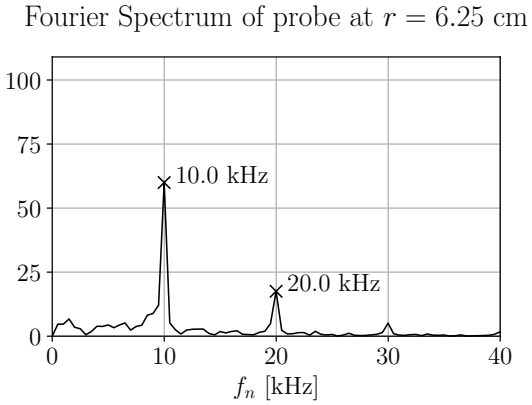

(b) Density reading from probe at $r = 6.25\,\mathrm{cm}$. Steady State with fit.

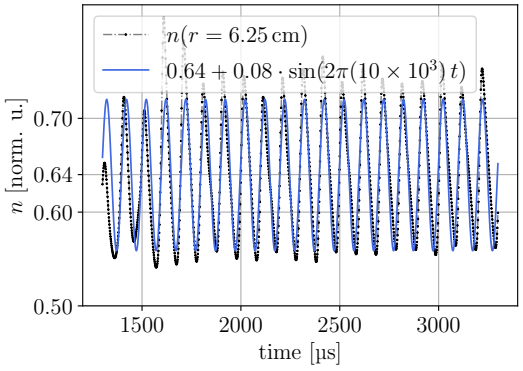

Figure 10

6 Conclusions

From the simulations we see that matter and energy is continuously transported out of the plasma. The transient behavour is nicely captured with radially propagating mushroom-shaped blobs, a buildup of a dipole in the plasma potential ϕ and a polarity in the vorticity. However, the most interesting result is that the steady state mechanism is different from what we originally expected in that we see two rotating centers rather than mushroom shaped blobs. The simulated probe observations show oscillating signals with a frequency of 10 kHz and relative amplitude of 12% of the signal mean value. It would be interesting to verify experimentally if changing the power of the heating source increases this frequency as we would expect from the simulations.

7 Partial Derivation of the ESEL Equations

The following section derive the first ESEL equation and gives the starting point for deriving the remaining two ESEL equations. More details are found in [7, 8]. The following references are also helpful in deriving the ESEL equations: [12, 14, 3, 9].

A multitude of different inelastic processes can be considered in the model, including:

- **Electron impact ionization (iz):** $\mathrm{He} + e^- \to \mathrm{He}^+ + 2e^-$.
- **Radiative recombination (rc):** $\mathrm{He}^+ + e^- \to \mathrm{He} + \gamma$.
- **Charge exchange collisions (cx):** $\mathrm{He} + \mathrm{He}^{+\,*} \to \mathrm{He}^+ + \mathrm{He}^*$. (Cold neutral + energetic ion → Cold ion + energetic neutral).

If the gas was H_2 and not He we should also consider:

- **Electron impact dissociation (dis):** $\mathrm{H}_2 + e^- \to 2\mathrm{H} + e^-$.
- **Molecular assisted ionization (m.iz):** $\mathrm{H}_2 + e^- \to \mathrm{H}_2^+ + 2e^- \to \mathrm{H} + \mathrm{H}^+ + 2e^-$.

7.1 Boltzmann Equation

Our starting point for developing a model of the plasma is the Boltzmann Equation

$$\partial_t f_\sigma + \dot{\mathbf{r}}_\sigma \cdot \boldsymbol{\nabla}_{\mathbf{r}} f_\sigma + \dot{\mathbf{v}}_\sigma \cdot \boldsymbol{\nabla}_{\mathbf{v}} f_\sigma = (\partial_t f_\sigma)^{\mathcal{C}} + (\partial_t f_\sigma)^{\mathcal{S}}. \tag{B.Eq.}$$

f_σ is the phase space distribution for species $\sigma \in \{e, i\}$ and $(\partial_t f_\sigma)^{\mathcal{C}}, (\partial_t f_\sigma)^{\mathcal{S}}$ are not actual time-differentials, but rather terms representing the change of the distribution function due to elastic and inelastic collisions respectively:

$$\begin{aligned}(\partial_t f_\sigma)^{\mathcal{C}} &= \sum_{\sigma' \neq \sigma} (\partial_t f_\sigma)^{\sigma'} \\ (\partial_t f_\sigma)^{\mathcal{S}} &= \sum_{\rho} (\partial_t f_\sigma)^{\rho}, \quad \rho \in \{\mathrm{iz}, \mathrm{rc}, \mathrm{m.iz}, \mathrm{cx}, \mathrm{dis}\}.\end{aligned}$$

The zeroth moment of the (B.Eq.) gives the continuity equation (unless otherwise noted, $\boldsymbol{\nabla}$ is with respect to $\mathbf{r}$):

$$\partial_t n_\sigma + \boldsymbol{\nabla} \cdot (n_\sigma \mathbf{u}_\sigma) = (\partial_t n_\sigma)^{\mathcal{S}}, \tag{C.Eq.}$$

where $\mathbf{u}_\sigma$ is the flow velocity and $(\partial_t n_\sigma)^{\mathcal{S}}$ are the density source terms from inelastic processes (see [14]):

$$\mathbf{u}_\sigma \equiv \langle \mathbf{v}_\sigma \rangle = \frac{1}{n_\sigma} \int \mathrm{d}\mathbf{v}_\sigma \, \mathbf{v}_\sigma f_\sigma.$$

$$(\partial_t n_e)^{\mathcal{S}} = (\partial_t n_e)^{\mathrm{iz}} + (\partial_t n_e)^{\mathrm{rc}} + (\partial_t n_e)^{\mathrm{m.iz}} = n_a n_e \langle \sigma_{\mathrm{iz}} \mathbf{v}_e \rangle - n_i n_e \langle \sigma_{\mathrm{rc}} \mathbf{v}_e \rangle + n_m n_e \langle \sigma_{\mathrm{m.iz}} \mathbf{v}_e \rangle . \tag{23a}$$

$$(\partial_t n_i)^{\mathcal{S}} = (\partial_t n_i)^{\mathrm{iz}} + (\partial_t n_i)^{\mathrm{rc}} + (\partial_t n_i)^{\mathrm{m.iz}}. \tag{23b}$$

To keep things general we let n_m be the density of molecules and n_a be the density of atoms. In our work, the gas is He (so we only have atoms, no molecules) which we assume to be ionised to first degree and we in general assume quasineutrality such that

$$n \equiv n_e \approx n_i, \tag{24a}$$

$$(\partial_t n)^{\mathcal{S}} \equiv (\partial_t n_e)^{\mathcal{S}} \approx (\partial_t n_i)^{\mathcal{S}}. \tag{24b}$$

The first moment of the (B.Eq.) gives the momentum equation:

$$n_\sigma m_\sigma \mathrm{d}_{t,\sigma} \mathbf{u}_\sigma = \sum_\alpha \mathbf{f}_\sigma^\alpha. \tag{M.Eq.}$$

Here $\mathbf{f}_\sigma^\alpha$ are all the force densities orginating from the (B.Eq.) and the elastic and inelastic sources:

$$\mathbf{f}_\sigma^d = -\boldsymbol{\nabla} p_\sigma, \quad \mathbf{f}_\sigma^E = q_\sigma n_\sigma \mathbf{E}, \quad \mathbf{f}_\sigma^B = q_\sigma n_\sigma \mathbf{u}_\sigma \times \mathbf{B}, \quad \mathbf{f}_\sigma^\pi = -\boldsymbol{\nabla} \cdot \boldsymbol{\pi}_\sigma, \tag{25a}$$

$$\mathbf{f}_e^R = \mathbf{f}_{ie}^R + \mathbf{f}_{ne}^R, \quad \mathbf{f}_i^R = \mathbf{f}_{ei}^R + \mathbf{f}_{ni}^R, \quad \text{where} \quad \mathbf{f}_{\sigma'\sigma}^R = m_\sigma \int \mathrm{d}\mathbf{v}_\sigma \, \mathbf{v}_\sigma (\partial_t n_\sigma)^{\sigma'}, \tag{25b}$$

$$\mathbf{f}_\sigma^{\mathcal{S}} = -m_\sigma \mathbf{u}_\sigma (\partial_t n_\sigma)^{\mathcal{S}}, \quad \mathbf{f}_e^\Gamma = m_e \mathbf{u}_m (\partial_t n_e)^{\mathrm{m.iz}} + m_e \mathbf{u}_a (\partial_t n_e)^{\mathrm{iz}}, \quad \mathbf{f}_i^\Gamma = \cdots . \tag{25c}$$

p_σ is the scalar pressure and $\boldsymbol{\pi}_\sigma$ is the generalised viscosity tensor, which together make up the pressure tensor:

$$p_\sigma \mathbf{1} + \boldsymbol{\pi}_\sigma = n_\sigma m_\sigma \left\langle (\mathbf{v}_\sigma - \mathbf{u}_\sigma)(\mathbf{v}_\sigma - \mathbf{u}_\sigma) \right\rangle ,$$

Note, $\mathbf{1}$ is the identity tensor and there is an implicit tensor/outer product between the two central velocities $(\mathbf{v}_\sigma - \mathbf{u}_\sigma)$ in the expression above.

7.2 Parallel and Perpendicular Equations

We wish to split the momentum equation into an equation parallel to the magnetic field $\mathbf{B}$ and an equation perpendicular to $\mathbf{B}$. As shown in the supplementary material, Section C, when splitting the advective term of the co-moving derivative we get the following

$$(\mathbf{u}_\sigma \cdot \boldsymbol{\nabla} \mathbf{u}_\sigma)_\parallel = \mathbf{u}_\sigma \cdot \boldsymbol{\nabla} \mathbf{u}_{\sigma,\parallel} + (\partial_t \mathbf{u}_\sigma)^{\mathrm{cf}},$$

where

$$(\partial_t \mathbf{u}_\sigma)^{\mathrm{cf}} \equiv -\mathbf{u}_\sigma \cdot \Big[\mathbf{u}_\sigma \cdot \Big(\hat{\mathbf{B}} \boldsymbol{\nabla} \Big) + \Big(\boldsymbol{\nabla} \hat{\mathbf{B}} \Big) \cdot \mathbf{u}_\sigma \Big] \hat{\mathbf{B}}.$$

cf stands for centrifugal and the reason for this will be clear shortly. In our geometry (See Section B of the supplementary material) the centrifugal advection is:

$$(\partial_t \mathbf{u}_\sigma)^{\mathrm{cf}} = \left(\frac{u_{\sigma,\parallel}^2}{R} \hat{\mathbf{R}} + \frac{u_{\sigma,R}\, u_{\sigma,\parallel}}{R} \hat{\mathbf{B}} \right). \tag{26}$$

From this we define the centrifugal force density:

$$\mathbf{f}^{\mathrm{cf}} \equiv m_\sigma n_\sigma (\partial_t \mathbf{u}_\sigma)^{\mathrm{cf}} = \frac{m_\sigma n_\sigma}{R} \Big(u_{\sigma,\parallel}^2 \hat{\mathbf{R}} + u_{\sigma,R} u_{\sigma,\parallel} \hat{\mathbf{B}} \Big). \tag{27}$$

Now, dividing the (M.Eq.) into it's parallel and perpendicular components gives:

$$\hat{\mathbf{B}}\hat{\mathbf{B}} \cdot (\text{M.Eq.}) \Rightarrow \frac{1}{\omega_{c\sigma}} \Big(\mathrm{d}_{t,\sigma} \mathbf{u}_{\sigma,\parallel} + (\partial_t \mathbf{u}_\sigma)^{\mathrm{cf}} \Big) = \sum_\alpha \frac{\mathbf{f}_{\sigma,\parallel}^\alpha}{n_\sigma q_\sigma B} \tag{28a}$$

$$\Big(\mathbf{1} - \hat{\mathbf{B}}\hat{\mathbf{B}} \Big) \cdot (\text{M.Eq.}) \Rightarrow \frac{1}{\omega_{c\sigma}} \Big(\mathrm{d}_{t,\sigma} \mathbf{u}_{\sigma,\perp} - (\partial_t \mathbf{u}_\sigma)^{\mathrm{cf}} \Big) = \sum_\alpha \frac{\mathbf{f}_{\sigma,\perp}^\alpha}{n_\sigma q_\sigma B}. \tag{28b}$$

7.3 Drift Ordering

We define the characteristic frequency $\partial_t \sim \omega_{\mathrm{char}}$ and the small parameter $\epsilon = \omega_{\mathrm{char}}/\omega_{ci0}$ and expand the perpendicular fluid velocity in this

$$\mathbf{u}_{\sigma,\perp} = \sum_i \epsilon^i \mathbf{u}_{\sigma,i} \approx \epsilon^0 \mathbf{u}_{\sigma,\perp,0} + \epsilon^1 \mathbf{u}_{\sigma,\perp,1}. \tag{29}$$

An order of magnitude estimate of the terms of Eq. (28b) is carried out in [12]. Grouping the terms by their ϵ-order gives:

$$\mathbf{0} = \overbrace{\left[\frac{1}{n_\sigma q_\sigma B}\left(\mathbf{f}^d_{\sigma,\perp} + \mathbf{f}^E_{\sigma,\perp} + \mathbf{f}^{\mathrm{cf}}_{\sigma,\perp}\right) + \mathbf{u}_{\sigma,\perp,0} \times \hat{\mathbf{B}}\right]}^{\epsilon^0} \tag{30}$$

$$+ \overbrace{\left[\frac{1}{n_\sigma q_\sigma B}\left(\mathbf{f}^p_\sigma + \mathbf{f}^\pi_\sigma + \mathbf{f}^R_\sigma + \mathbf{f}^n_{\sigma,0} + \mathbf{f}^\Gamma_{\sigma,0}\right) + \mathbf{u}_{\sigma,\perp,1} \times \hat{\mathbf{B}}\right]}^{\epsilon^1} \tag{31}$$

$$+ \cdots \tag{32}$$

where we have introduced the polarisation force density:

$$\mathbf{f}^p_\sigma = -m_\sigma n_\sigma \mathrm{d}^1_{t,\sigma} \mathbf{u}_{\sigma,\perp,0}, \quad \text{where} \quad \mathrm{d}^1_{t,\sigma} \equiv \partial_t + \left(\mathbf{u}_{\sigma,\perp,0} + \mathbf{u}_{\sigma,\parallel}\right) \cdot \boldsymbol{\nabla} \tag{33}$$

By crossing the zeroth order equation with $\hat{\mathbf{B}}$ and using $-\left(\mathbf{a} \times \hat{\mathbf{B}}\right) \times \hat{\mathbf{B}} = \mathbf{a}$ we get the zeroth order drift:

$$\mathbf{u}_{\sigma,\perp,0} = \mathbf{u}^E_\perp + \mathbf{u}^d_{\sigma,\perp} + \mathbf{u}^{\mathrm{cf}}_{\sigma,\perp}, \tag{34a}$$

$$\mathbf{u}^E_\perp = \frac{\mathbf{E}_\perp \times \hat{\mathbf{B}}}{B} \approx -\frac{\boldsymbol{\nabla}_\perp \phi \times \hat{\mathbf{B}}}{B}, \quad \mathbf{u}^d_{\sigma,\perp} = -\frac{\boldsymbol{\nabla}_\perp p_\sigma \times \hat{\mathbf{B}}}{n_\sigma q_\sigma B}, \quad \mathbf{u}^{\mathrm{cf}}_{\sigma,\perp} = \frac{\mathbf{f}^{\mathrm{cf}}_{\sigma,\perp} \times \hat{\mathbf{B}}}{n_\sigma q_\sigma B} = \frac{m_\sigma u^2_{\sigma,\parallel}}{R} \frac{\hat{\mathbf{R}} \times \hat{\mathbf{B}}}{q_\sigma B}, \tag{34b}$$

where we also applied the electrostatic approximation $\mathbf{E}_\perp \approx -\boldsymbol{\nabla}_\perp \phi$ and note that the $\mathbf{E} \times \mathbf{B}$ drift is independent of the species. Focusing on the first order equation and using the same trick as before gives the first order drift:

$$\mathbf{u}_{\sigma,\perp,1} = \mathbf{u}^p_{\sigma,\perp} + \mathbf{u}^\pi_{\sigma,\perp} + \mathbf{u}^R_{\sigma,\perp} + \mathbf{u}^{\mathcal{S}}_{\sigma,\perp} + \mathbf{u}^\Gamma_{\sigma,\perp}, \tag{35a}$$

$$\text{where } \mathbf{u}^\alpha_{\sigma,\perp} = \frac{\mathbf{f}^\alpha_{\sigma,\perp} \times \hat{\mathbf{B}}}{n_\sigma q_\sigma B}, \quad \alpha \in \{p, \pi, R, \mathcal{S}, \Gamma\}. \tag{35b}$$

7.4 Curvature Operator

We introduce the curvature operator acting on any field $\varphi(\mathbf{r}, \mathbf{t})$:

$$\mathcal{C}(\varphi) = \boldsymbol{\nabla} \cdot \left(\frac{-\boldsymbol{\nabla}_\perp \varphi \times \hat{\mathbf{B}}}{B}\right) = \frac{\left(\boldsymbol{\nabla} \times \hat{\mathbf{B}}\right) \cdot \boldsymbol{\nabla}\varphi}{B} + \left(\boldsymbol{\nabla} \frac{1}{B}\right) \cdot \left(\hat{\mathbf{B}} \times \boldsymbol{\nabla}\varphi\right).$$

Note, that $\mathcal{C}(\varphi)$ is zero for a constant magnetic field. As shown in Section D of the supplementary material, in our geometry, where the $\mathbf{B}$-field is given by (1), the curvature operator simplifies to a vertical derivative:

$$\mathcal{C}(\varphi) = \frac{2}{B_0 R_0} \partial_z \varphi = \frac{2}{B_0 R_0} \left(\sin(\theta)\partial_r + \frac{\cos(\theta)}{r}\partial_\theta\right)\varphi.$$

7.5 The Density Equation

To arrive at the density equation of the ESEL equations, we assume quasineutrality, Eq. (24), and substitute the drifts up to first order from Eqs. (34) and (35) into the (C.Eq.):

$$\partial_t n + \boldsymbol{\nabla} \cdot \left(n \mathbf{u}_{\sigma,\parallel}\right) + \sum_\alpha \boldsymbol{\nabla} \cdot \left(n \mathbf{u}^\alpha_{\sigma,\perp}\right) = (\partial_t n)^{\mathcal{S}}, \qquad \alpha \in \{E, d, \mathrm{cf}, p, \pi, R, \mathcal{S}, \Gamma\} \tag{36}$$

Since we have assumed quasineutrality and in this work are mainly interested in the electron density, we will focus on the electron equation. At this point, we apply an arsenal of approximations:

$$\mathbf{u}_{e,\perp}^{\pi} = \mathcal{O}(\epsilon^2) \approx \mathbf{0} \qquad \text{(viscosity is of order } \epsilon^2 \text{ and therefore negligible).}$$

$$\mathbf{u}_{e,\perp}^{p}, \mathbf{u}_{e,\perp}^{\mathcal{S}}, \mathbf{u}_{e,\perp}^{\Gamma} \propto \frac{1}{\omega_{ce}} \approx \mathbf{0} \qquad (m_e \text{ is small, so these drifts are negligible}).$$

$$\mathbf{u}_{e,\perp}^{\mathrm{cf}} = -\frac{m_e u_{e,\parallel}^2}{R} \frac{\hat{\mathbf{R}} \times \hat{\mathbf{B}}}{eB} = \mathbf{0} \quad \text{(symmetry of NORTH gives no parallel net flow } \mathbf{u}_{e,\parallel} = \mathbf{0}).$$

With these approximations only the $\mathbf{E} \times \mathbf{B}$, diamagnetic and collision drifts remain in the perpendicular velocity:

$$\mathbf{u}_{e,\perp} \approx \mathbf{u}_{\perp}^{E} + \mathbf{u}_{e,\perp}^{d} + \mathbf{u}_{e,\perp}^{R}.$$

From the definition of the drifts, Eq. (34), and of the curvature operator, Eq. (66), follows:

$$\boldsymbol{\nabla} \cdot \left(n \mathbf{u}_{\perp}^{E}\right) = \mathbf{u}_{\perp}^{E} \cdot \boldsymbol{\nabla} n + n \mathcal{C}(\phi), \qquad \boldsymbol{\nabla} \cdot \left(n \mathbf{u}_{e,\perp}^{d}\right) = -\frac{1}{e} \mathcal{C}(p_e) = -\frac{1}{e} \mathcal{C}(n T_e).$$

Inserting this in Eq. (36) gives the ESEL density equation:

$$\mathrm{d}_t^E n + n \mathcal{C}(\phi) - \frac{1}{e} \mathcal{C}(n T_e) = (\partial_t n_e)^{\mathcal{S}} + (\partial_t n_e)^{\mathcal{L}}, \tag{37}$$

where we have introduced the low order co-moving derivative and the density loss term:

$$\mathrm{d}_t^E \equiv \partial_t + \mathbf{u}_{\sigma,\perp}^{E} \cdot \boldsymbol{\nabla}, \tag{38}$$

$$(\partial_t n_e)^{\mathcal{L}} \equiv -\boldsymbol{\nabla} \cdot \left(n \mathbf{u}_{e,\perp}^{R}\right) - \boldsymbol{\nabla} \cdot \left(n \mathbf{u}_{e,\parallel}\right). \tag{39}$$

7.5.1 Diffusion

As shown in Section F of the supplementary material the divergence of the friction flux in Eq. (39) gives rise to two diffusion terms from ion-electron and atom-electron collisions respectively:

$$-\boldsymbol{\nabla} \cdot \left(n \mathbf{u}_{e,\perp}^{R}\right) = -\boldsymbol{\nabla} \cdot \left(n \mathbf{u}_{ie,\perp}^{R}\right) - \boldsymbol{\nabla} \cdot \left(n \mathbf{u}_{ae,\perp}^{R}\right), \quad \text{where} \tag{40a}$$

$$-\boldsymbol{\nabla} \cdot \left(n \mathbf{u}_{ie,\perp}^{R}\right) \approx \left(1 + \frac{T_i}{T_e}\right) \boldsymbol{\nabla} \cdot (D_{ei} \boldsymbol{\nabla}_{\perp} n). \tag{40b}$$

$$-\boldsymbol{\nabla} \cdot \left(n \mathbf{u}_{ae,\perp}^{R}\right)) \approx D_{ea} \left(1 + \frac{T_i}{T_e}\right) \nabla_{\perp}^2 n. \tag{40c}$$

The diffusion coefficients are taken from [10] and are estimated from the characteristic scales of the system (n_0, T_{e0}, B_0):

$$D_{ei} \equiv \nu_{ei0}\, \rho_{Le0}^2 \equiv k_{ei}\, n\, \rho_{Le0}^2, \tag{41a}$$

$$\rho_{Le0}^2 \equiv \frac{m_e T_{e0}}{e^2 B_0^2} \quad k_{ei} \equiv \frac{2^{1/2} Z^2 e^4 \ln \Lambda_0}{12 \pi^{3/2} e_0^2 m_e^{1/2} T_{e0}^{3/2}}, \quad \ln \Lambda_0 \equiv \ln\left(\frac{12 \pi n_0 \lambda_{D0}^3}{Z}\right), \quad \lambda_{D0} \equiv \sqrt{\frac{\varepsilon_0 T_{e0}}{n_0 e^2}}. \tag{41b}$$

$$D_{ea} \equiv \nu_{ea0}\, \rho_{Le0}^2. \tag{42a}$$

$$\rho_{Le0}^2 \equiv \frac{m_e T_{e0}}{e^2 B_0^2} \quad \nu_{ea0} = \frac{8\sqrt{2}}{3\sqrt{\pi}} n_{a0} \sqrt{\frac{T_{e0}}{m_e}} \sigma_{ea}, \quad n_{a0} = 1.2 \cdot 10^{19}\,\mathrm{m}^{-3}, \quad \sigma_{ea} = 6 \times 10^{-21}\,\mathrm{m}^2. \tag{42b}$$

σ_{ea} is the elastic collision cross section between the electron and neutral atoms in the plasma. According to [11], the cross section has a value of $6 \times 10^{-21}\,\mathrm{m}^2$ at an electron temperature of $T_e = T_{e0} = 10\,\mathrm{eV}$. The density of neutral atoms n_{a0} is estimated from the typical He gas pressure in NORTH which is on the order of $5 \cdot 10^{-4}$ mbar corresponding to a particle density of $\sim 1.2 \cdot 10^{19}\,\mathrm{m}^{-3}$.

7.6 The Vorticity Equation

By adding the (C.Eq.) of each species times the species charge q_σ we immediately arrive at the charge continuity equation:

$$\sum_\sigma q_\sigma (\text{C.Eq.})_\sigma \Leftrightarrow \sum_\sigma q_\sigma \partial_t n_\sigma + \boldsymbol{\nabla} \cdot (n_\sigma q_\sigma \mathbf{u}_\sigma) = \sum_\sigma q_\sigma (\partial_t n_\sigma)^{\mathcal{S}} \Leftrightarrow$$
$$\boldsymbol{\nabla} \cdot \mathbf{J} = \sum_\sigma q_\sigma \Big[\partial_t n_\sigma + (\partial_t n_\sigma)^{\mathcal{S}} \Big], \tag{43}$$

where we have defined the current density in the natural way:

$$\mathbf{J} = \sum_\sigma n_\sigma q_\sigma \mathbf{u}_\sigma.$$

We assume we only have first ionization ($q_i = e, q_e = -e$) and that the quasineutrality of Eq. (24) applies. In this regime, Eq. (43) simplifies to the magnetostatic charge continuity equation:

$$\boldsymbol{\nabla} \cdot \mathbf{J} = 0. \tag{44}$$

This is as far I got in the derivation of the ESEL equations. From the equation above it is possible to obtain the vorticity equation. An important step in this is the thin-layer approximation which assumes local density variations in the domain to be neglible compared to the variation in the macroscopic background equilibrium density [12].

Finally from the second moment of the (B.Eq.) one obtains an energy equation which leads to the temperature equation of the ESEL model.

A Supplementary Material

A.1 Useful Tensor and Dyadic Rules

For convenience we quickly reiterate some useful tensor and vector calculus rules. Most of the rules are taken from [9, p. 53]. We use implicit outer products between tensors such that $\mathbf{ab} = \mathbf{a} \otimes \mathbf{b}$. For all $\mathbf{a}, \mathbf{b}, \mathbf{c}, \mathbf{d} \in \mathbb{R}^3$ and $\alpha \in \mathbb{R}$, we have

$$(\mathbf{a} \cdot \mathbf{bc}) = ((\mathbf{a} \cdot \mathbf{b})\mathbf{c}) \quad \text{Definition of dyad (outer prod.)} \tag{45a}$$

$$(\mathbf{ab} \cdot \mathbf{c}) = (\mathbf{a}(\mathbf{b} \cdot \mathbf{c})) \quad \text{Definition of dyad (outer prod.)} \tag{45b}$$

$$(\mathbf{a} \cdot \mathbf{bc}) \cdot \mathbf{d} = \mathbf{a} \cdot (\mathbf{bc} \cdot \mathbf{d}) \quad \text{Associativity of dot product} \tag{45c}$$

$$(\mathbf{a} \cdot \boldsymbol{\nabla}\mathbf{c}) \cdot \mathbf{d} = \mathbf{a} \cdot ((\boldsymbol{\nabla}\mathbf{c}) \cdot \mathbf{d}) \quad \text{also true with grad (grad only acts on } \mathbf{c}) \tag{45d}$$

$$(\mathbf{a} \cdot \mathbf{bc})\mathbf{d} = (\mathbf{a} \cdot \mathbf{b})\mathbf{cd} \quad \text{Associativity of outer product} \tag{45e}$$

$$\boldsymbol{\nabla} \cdot (\mathbf{ab}) = \mathbf{a} \cdot \boldsymbol{\nabla}\mathbf{b} + (\boldsymbol{\nabla} \cdot \mathbf{a})\mathbf{b} \quad \text{Divergence of dyad [9, T.10, p. 53]} \tag{45f}$$

$$\boldsymbol{\nabla}(\mathbf{a} \cdot \mathbf{b}) = (\boldsymbol{\nabla}\mathbf{a}) \cdot \mathbf{b} + (\boldsymbol{\nabla}\mathbf{b}) \cdot \mathbf{a} \quad \text{Dot product rule [9, T.18, p. 53]} \tag{45g}$$

$$\boldsymbol{\nabla}(\alpha\mathbf{a}) = (\boldsymbol{\nabla}\alpha)\mathbf{a} + \alpha\boldsymbol{\nabla}\mathbf{a} \quad \text{Scaled vector product rule} \tag{45h}$$

$$\boldsymbol{\nabla} \cdot (\alpha\mathbf{a}) = \alpha\boldsymbol{\nabla} \cdot \mathbf{a} + \mathbf{a} \cdot \boldsymbol{\nabla}\alpha \quad \text{Divergence scaled vector product rule} \tag{45i}$$

$$\boldsymbol{\nabla} \cdot (\mathbf{a} \times \mathbf{b}) = (\boldsymbol{\nabla} \times \mathbf{a}) \cdot \mathbf{b} - \mathbf{a} \cdot (\boldsymbol{\nabla} \times \mathbf{b}) \quad \text{Divergence cross product rule} \tag{45j}$$

$$\boldsymbol{\nabla} \times (\alpha\mathbf{a}) = \alpha(\boldsymbol{\nabla} \times \mathbf{a}) + (\boldsymbol{\nabla}\alpha) \times \mathbf{a} \quad \text{Curl scaled vector product rule} \tag{45k}$$

$$\boldsymbol{\nabla} \times (\mathbf{a} \times \mathbf{b}) = \boldsymbol{\nabla} \cdot (\mathbf{ba} - \mathbf{ab}) \quad \text{Curl cross product rule [9, T.16, p. 53]} \tag{45l}$$

B Magnetic Field Geometry

B.1 Toroidal Coordinate System

In the following we calculate the metric tensor and Jacobian of the toroidal coordinate transformation. This is used as input to the BOUT++ simulation and for calculating e.g. volume integrals in the data analysis. Any position vector $\mathbf{R}$ with cartesian coordinates (x, y, z) can be expressed in the curvilinear coordinate system through the transformation:

$$\mathbf{R}(r, \zeta, \theta) = \begin{pmatrix} x \\ y \\ z \end{pmatrix} = \begin{pmatrix} (R_0 + r\cos\theta)\cos\zeta \\ (R_0 + r\cos\theta)\sin\zeta \\ r\sin\theta \end{pmatrix}, \tag{46}$$

where, again, $R_0 = 0.25\,\mathrm{m}$ is the major radius of North. The total derivative (Jacobian matrix) of the transformation is

$$D\,\mathbf{R} = \begin{pmatrix} \partial_r\mathbf{R} & \partial_\zeta\mathbf{R} & \partial_\theta\mathbf{R} \end{pmatrix} = \tag{47}$$

$$\begin{pmatrix} \cos\theta\cos\zeta & -(R_0 + r\cos\theta)\sin\zeta & -r\sin\theta\cos\zeta \\ \cos\theta\sin\zeta & (R_0 + r\cos\theta)\cos\zeta & -r\sin\theta\sin\zeta \\ \sin\theta & 0 & r\cos\theta \end{pmatrix} \tag{48}$$

The covariant and contravariant basis vectors are respectively defined by

$$\mathbf{e}_i = \frac{\partial\mathbf{R}}{\partial u^i}, \qquad \mathbf{e}^i = \boldsymbol{\nabla}u^i. \tag{49}$$

Thus, the covariant basis is identified as the columns of the total derivative (48), and a basis vector such as $\mathbf{e}_1$ is the tangent vector to the curve which emerges when keeping the other two parameters, $u^2 = \zeta$ and $u^3 = \theta$ fixed. The contravariant basis can be obtained by inverting the transformation $\mathbf{R}(r, \zeta, \theta)$. From these bases we get the co- and contravariant metric tensors:

$$g_{ij} = \mathbf{e}_i \cdot \mathbf{e}_j, \qquad g^{ij} = \mathbf{e}^i \cdot \mathbf{e}^j.$$

The matrix representation $\mathbf{g}$ of the covariant metric g_{ij} can also be obtained directly from the total derivate (48):

$$\mathbf{g} = (D\,\mathbf{R})^T (D\,\mathbf{R}) = \begin{pmatrix} 1 & 0 & 0 \\ 0 & (R_0 + r\cos\theta)^2 & 0 \\ 0 & 0 & r^2 \end{pmatrix}. \tag{50}$$

Finally, the inverse matrix $\mathbf{g}^{-1}$ represents the contravariant metric g^{ij}. Together, these metric coefficients determine how to switch back and forth between co- and contravariant components of a vector [9]. Furthermore, from g_{ij} we obtain the Jacobian[1] $J = \partial_r \mathbf{R} \cdot (\partial_\zeta \mathbf{R} \times \partial_\theta \mathbf{R})$ explaining how much volume elements are stretched by the curvilinear transformation:

$$J(r, \zeta, \theta) = \sqrt{\det[g_{ij}]} = r(R_0 + r\cos\theta). \tag{51}$$

With the metric tensors and Jacobian at hand, we have the necessary machinery for working in the toroidal coordinate system, which we have used in the model.

B.2 Cylindrical Coordinate System

In this section, we work with the cylindrical coordinates: $(u^1, u^2, u^3) = (R, \zeta, z)$. Any position vector $\mathbf{X}$ with cartesian coordinates (x, y, z) can be expressed in the curvilinear coordinate system through the transformation:

$$\mathbf{X}(r, \zeta, \theta) = \begin{pmatrix} x \\ y \\ z \end{pmatrix} = \begin{pmatrix} R\cos\zeta \\ R\sin\zeta \\ z \end{pmatrix}. \tag{52}$$

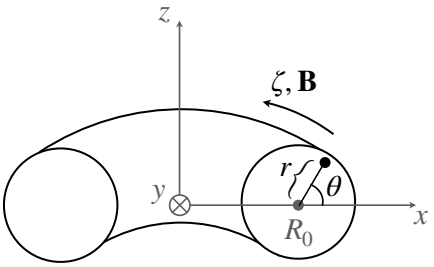

Figure 11: Illustration of toroidal curvilinear coordinates. Instead of (r, ζ, θ), in this section we work with the cylindrical coordinates (R, ζ, z).

The covariant and contravariant basis vectors are respectively defined by

$$\mathbf{e}_i = \frac{\partial \mathbf{R}}{\partial u^i}, \qquad \mathbf{e}^i = \boldsymbol{\nabla} u^i = \frac{\mathbf{e}_j \times \mathbf{e}_k}{\mathbf{e}_i \cdot (\mathbf{e}_j \times \mathbf{e}_k)}. \tag{53}$$

So in a cartesian representation, the bases are:

$$\mathbf{e}_R = \frac{\partial \mathbf{X}}{\partial R} = \begin{pmatrix} \cos\zeta \\ \sin\zeta \\ 0 \end{pmatrix}, \qquad \mathbf{e}_\zeta = \frac{\partial \mathbf{X}}{\partial \zeta} = R \begin{pmatrix} -\sin\zeta \\ \cos\zeta \\ 0 \end{pmatrix}, \qquad \mathbf{e}_z = \frac{\partial \mathbf{X}}{\partial z} = \begin{pmatrix} 0 \\ 0 \\ 1 \end{pmatrix} \tag{54}$$

$$\mathbf{e}^R = \begin{pmatrix} \cos\zeta \\ \sin\zeta \\ 0 \end{pmatrix}, \qquad \mathbf{e}^\zeta = \frac{1}{R} \begin{pmatrix} -\sin(\theta) \\ \cos\zeta \\ 0 \end{pmatrix}, \qquad \mathbf{e}^z = \begin{pmatrix} 0 \\ 0 \\ 1 \end{pmatrix} \tag{55}$$

One can confirm that

$$\mathbf{e}^i \cdot \mathbf{e}_j = \delta^i_j$$

[1] We reserve the simple name "Jacobian" for this quantity, which could also be calculated as the determinant of the "Jacobian matrix": $J = \det[D\,\mathbf{R}]$.

Note, that we can normalise the basises to get the familiar well-known unit vectors in cylindrical coordinates: $\hat{\mathbf{i}} = \mathbf{e}_i |\mathbf{e}_i|^{-1} = \mathbf{e}^i \big|\mathbf{e}^i\big|^{-1}$. The gradient therefore becomes:

$$\boldsymbol{\nabla} = \boldsymbol{\nabla} u^i \frac{\partial}{\partial u^i} = \mathbf{e}^i \frac{\partial}{\partial u^i} = \left(\mathbf{e}^R \frac{\partial}{\partial R} + \mathbf{e}^\zeta \frac{\partial}{\partial \zeta} + \mathbf{e}^z \frac{\partial}{\partial z} \right) = \left(\hat{\mathbf{R}} \frac{\partial}{\partial R} + \hat{\boldsymbol{\zeta}} \frac{1}{R} \frac{\partial}{\partial \zeta} + \hat{\mathbf{z}} \frac{\partial}{\partial z} \right). \tag{56}$$

B.3 B-Field

From Ampere's law the $\mathbf{B}$-field is (where N is number of current loops and I is current through each loop):

$$\mathbf{B} = \frac{\mu_0 N I}{2\pi R} \hat{\boldsymbol{\zeta}} \equiv \frac{B_0 R_0}{R} \hat{\boldsymbol{\zeta}}, \tag{57}$$

where, $R_0 = 0.25\,\mathrm{m}$ is the major radius of North and B_0 is the B-field at $R = R_0$. So the unit direction vector $\hat{\mathbf{B}}$ is:

$$\hat{\mathbf{B}} = \hat{\boldsymbol{\zeta}} = \frac{1}{R} \mathbf{e}_\zeta = R\, \mathbf{e}^\zeta$$

C Parallel and perpendicular component of advective term

Let $\mathbf{u} = \langle \mathbf{v} \rangle$ denote the fluid velocity, and $\mathbf{a} = \mathbf{a}(\mathbf{r}, t)$ be any vector field which depend on position and time. Then the parallel component of the advective derivative of $\mathbf{a}$ is:

$$\begin{aligned}
(\mathbf{u} \cdot \boldsymbol{\nabla} \mathbf{a})_\parallel &= (\mathbf{u} \cdot \boldsymbol{\nabla} \mathbf{a}) \cdot \hat{\mathbf{B}} \hat{\mathbf{B}} \\
&= \Big(\mathbf{u} \cdot \Big((\boldsymbol{\nabla} \mathbf{a}) \cdot \hat{\mathbf{B}} \Big) \Big) \hat{\mathbf{B}} && \text{using (45d)} \\
&= \Big(\mathbf{u} \cdot \Big[\boldsymbol{\nabla} \Big(\mathbf{a} \cdot \hat{\mathbf{B}} \Big) - \Big(\boldsymbol{\nabla} \hat{\mathbf{B}} \Big) \cdot \mathbf{a} \Big] \Big) \hat{\mathbf{B}} && \text{using (45g)} \\
&= \mathbf{u} \cdot \Big(\Big[\boldsymbol{\nabla} \Big(\mathbf{a} \cdot \hat{\mathbf{B}} \Big) \Big] \hat{\mathbf{B}} - \Big[\Big(\boldsymbol{\nabla} \hat{\mathbf{B}} \Big) \cdot \mathbf{a} \Big] \hat{\mathbf{B}} \Big) && \text{using (45a)} \\
&= \mathbf{u} \cdot \Big\{ \boldsymbol{\nabla} \Big(\mathbf{a} \cdot \hat{\mathbf{B}} \hat{\mathbf{B}} \Big) - (\mathbf{a} \cdot \hat{\mathbf{B}}) \boldsymbol{\nabla} \hat{\mathbf{B}} - \Big[\Big(\boldsymbol{\nabla} \hat{\mathbf{B}} \Big) \cdot \mathbf{a} \Big] \hat{\mathbf{B}} \Big\} && \text{using (45h), (45a)} \\
&= \mathbf{u} \cdot \boldsymbol{\nabla} \mathbf{a}_\parallel - \mathbf{u} \cdot \Big[\mathbf{a} \cdot \Big(\hat{\mathbf{B}} \boldsymbol{\nabla} \Big) + \Big(\boldsymbol{\nabla} \hat{\mathbf{B}} \Big) \cdot \mathbf{a} \Big] \hat{\mathbf{B}} && \text{using (45e), (45a)}
\end{aligned}$$

The result motivates us to define the advective time-derivative due to the curvature of the $\mathbf{B}$-field:

$$(\partial_t \mathbf{u}_\sigma)^{\mathrm{cf}} \equiv -\mathbf{u}_\sigma \cdot \Big[\mathbf{u}_\sigma \cdot \Big(\hat{\mathbf{B}} \boldsymbol{\nabla} \Big) + \Big(\boldsymbol{\nabla} \hat{\mathbf{B}} \Big) \cdot \mathbf{u}_\sigma \Big] \hat{\mathbf{B}}. \tag{59}$$

The cf stands for centrifugal, as the advection gives rise to a centrifugal drift. By using that $\mathbf{a}_\perp = \mathbf{a} - \mathbf{a}_\parallel$ we can determine the perpendicular component of the advective term:

$$(\mathbf{u} \cdot \boldsymbol{\nabla} \mathbf{a})_\perp = \mathbf{u} \cdot \boldsymbol{\nabla} \mathbf{a} - (\mathbf{u} \cdot \boldsymbol{\nabla} \mathbf{a})_\parallel = \mathbf{u} \cdot \boldsymbol{\nabla} \mathbf{a}_\perp + \mathbf{u} \cdot \Big[\mathbf{a} \cdot \Big(\hat{\mathbf{B}} \boldsymbol{\nabla} \Big) + \Big(\boldsymbol{\nabla} \hat{\mathbf{B}} \Big) \cdot \mathbf{a} \Big] \hat{\mathbf{B}}$$

If we want, we can also write this without any outer products:

$$(\mathbf{u} \cdot \boldsymbol{\nabla} \mathbf{a})_\perp = (\mathbf{u} \cdot \boldsymbol{\nabla}) \mathbf{a}_\perp + \Big(\mathbf{a} \cdot \hat{\mathbf{B}} \Big) (\mathbf{u} \cdot \boldsymbol{\nabla}) \hat{\mathbf{B}} + \Big[\mathbf{a} \cdot \Big((\mathbf{u} \cdot \boldsymbol{\nabla}) \hat{\mathbf{B}} \Big) \Big] \hat{\mathbf{B}}$$

C.1 Advection in our geometry

In our geometry, we have:

$$\frac{\partial}{\partial \zeta} \hat{\mathbf{B}} = \frac{\partial}{\partial \zeta} \hat{\boldsymbol{\zeta}} = \frac{\partial}{\partial \zeta} \begin{pmatrix} -\sin \zeta \\ \cos \zeta \\ 0 \end{pmatrix} = - \begin{pmatrix} \cos \zeta \\ \sin \zeta \\ 0 \end{pmatrix} = -\hat{\mathbf{R}}.$$

The first non-trivial term in the perpendicular advection therefore is:

$$\Big(\mathbf{u}\cdot\hat{\mathbf{B}}\Big)(\mathbf{u}\cdot\boldsymbol{\nabla})\hat{\mathbf{B}} = \Big(\mathbf{u}\cdot\hat{\mathbf{B}}\Big)\left(u^R\frac{\partial}{\partial R}+u^\zeta\frac{\partial}{\partial\zeta}+u^z\frac{\partial}{\partial z}\right)\hat{\mathbf{B}} = -\Big(\mathbf{u}\cdot\hat{\mathbf{B}}\Big)(\mathbf{u}\cdot\mathbf{e}_\zeta)\hat{\mathbf{R}}$$
$$= -\frac{1}{R}\Big(\mathbf{u}\cdot\hat{\mathbf{B}}\Big)\Big(\mathbf{u}\cdot\hat{\mathbf{B}}\Big)\hat{\mathbf{R}} = -\frac{u_\parallel^2}{R}\hat{\mathbf{R}}.$$

For the second term we need to calculate the outer product of the gradient and B-field unit vector, $\boldsymbol{\nabla}\hat{\mathbf{B}}$:

$$\boldsymbol{\nabla}\hat{\mathbf{B}} = \boldsymbol{\nabla}\hat{\boldsymbol{\zeta}} = \left(\hat{\mathbf{R}}\frac{\partial}{\partial R}+\hat{\boldsymbol{\zeta}}\frac{1}{R}\frac{\partial}{\partial\zeta}+\hat{\mathbf{z}}\frac{\partial}{\partial z}\right)\hat{\boldsymbol{\zeta}} = -\frac{1}{R}\hat{\boldsymbol{\zeta}}\hat{\mathbf{R}}. \tag{60}$$

So, the second term is:

$$\mathbf{u}\cdot(\boldsymbol{\nabla}\mathbf{b}\cdot\mathbf{u})\hat{\mathbf{B}} = -\frac{1}{R}\mathbf{u}\cdot\Big(\hat{\boldsymbol{\zeta}}\hat{\mathbf{R}}\cdot\mathbf{u}\Big)\hat{\mathbf{B}} = -\frac{u_R\,u_\parallel}{R}\hat{\mathbf{B}}.$$

To summarise, the parallel and perpendicular advection in our geometry is:

$$(\mathbf{u}\cdot\boldsymbol{\nabla}\mathbf{u})_\parallel = \mathbf{u}\cdot\boldsymbol{\nabla}\mathbf{u}_\parallel + \left(\frac{u_\parallel^2}{R}\hat{\mathbf{R}}+\frac{u_R\,u_\parallel}{R}\hat{\mathbf{B}}\right) \tag{61a}$$

$$(\mathbf{u}\cdot\boldsymbol{\nabla}\mathbf{u})_\perp = \mathbf{u}\cdot\boldsymbol{\nabla}\mathbf{u}_\perp - \left(\frac{u_\parallel^2}{R}\hat{\mathbf{R}}+\frac{u_R\,u_\parallel}{R}\hat{\mathbf{B}}\right). \tag{61b}$$

In other words, in our geometry we have:

$$(\partial_t\mathbf{u}_\sigma)^{\mathrm{cf}} = \left(\frac{u_{\sigma,\parallel}^2}{R}\hat{\mathbf{R}}+\frac{u_{\sigma,R}\,u_{\sigma,\parallel}}{R}\hat{\mathbf{B}}\right). \tag{62}$$

D Curvature Operator

We define the curvature operator acting on any field $\varphi(\mathbf{r},\mathbf{t})$ as:

$$\begin{aligned}
\mathcal{C}(\varphi) &\equiv \boldsymbol{\nabla}\cdot\left(\frac{-(\boldsymbol{\nabla}_\perp\varphi)\times\hat{\mathbf{B}}}{B}\right)\\
&= \frac{\boldsymbol{\nabla}\cdot\Big(\hat{\mathbf{B}}\times\boldsymbol{\nabla}\varphi\Big)}{B}+\left(\boldsymbol{\nabla}\frac{1}{B}\right)\cdot\Big(\hat{\mathbf{B}}\times\boldsymbol{\nabla}\varphi\Big) && \text{using (45i)}\\
&= \frac{\Big(\boldsymbol{\nabla}\times\hat{\mathbf{B}}\Big)\cdot\boldsymbol{\nabla}\varphi}{B}+\frac{\hat{\mathbf{B}}\cdot(\boldsymbol{\nabla}\times\boldsymbol{\nabla}\varphi)}{B}+\left(\boldsymbol{\nabla}\frac{1}{B}\right)\cdot\Big(\hat{\mathbf{B}}\times\boldsymbol{\nabla}\varphi\Big) && \text{using (45j)}\\
&= \frac{\Big(\boldsymbol{\nabla}\times\hat{\mathbf{B}}\Big)\cdot\boldsymbol{\nabla}\varphi}{B}+\left(\boldsymbol{\nabla}\frac{1}{B}\right)\cdot\Big(\hat{\mathbf{B}}\times\boldsymbol{\nabla}\varphi\Big). && \text{since } \boldsymbol{\nabla}\times\boldsymbol{\nabla}\varphi=\mathbf{0}
\end{aligned}$$

In our geometry where $\mathbf{B}$ is given by Eq. (57), we have

$$\boldsymbol{\nabla}\left(\frac{1}{B}\right) = \frac{1}{B_0R_0}\boldsymbol{\nabla}(R) = \frac{1}{B_0R_0}\hat{\mathbf{R}}. \tag{64}$$

Using the vector identity $\hat{\mathbf{R}}\cdot(\hat{\mathbf{B}}\times\boldsymbol{\nabla}\varphi) = \boldsymbol{\nabla}\varphi\cdot(\hat{\mathbf{R}}\times\hat{\mathbf{B}})$ gives

$$\boldsymbol{\nabla}\left(\frac{1}{B}\right)\cdot\Big(\hat{\mathbf{B}}\times\boldsymbol{\nabla}\varphi\Big) = \frac{1}{B_0R_0}\boldsymbol{\nabla}\varphi\cdot\Big(\hat{\mathbf{R}}\times\hat{\mathbf{B}}\Big) = \frac{1}{B_0R_0}\hat{\mathbf{z}}\cdot\boldsymbol{\nabla}\varphi.$$

Meanwhile the curl of $\hat{\mathbf{B}} = \hat{\boldsymbol{\zeta}}$ (in cylindrical coordinates R,ζ,z) is

$$\boldsymbol{\nabla}\times\hat{\mathbf{B}} = \frac{1}{R}\partial_R(R)\;\hat{\mathbf{z}} = \frac{1}{R}\hat{\mathbf{z}}. \tag{65}$$

Putting everything together reduces the curvature operator to:

$$\mathcal{C}(\varphi) = \frac{2}{B_0 R_0}\hat{\mathbf{z}} \cdot \boldsymbol{\nabla}\varphi = \frac{2}{B_0 R_0}\partial_z \varphi, \tag{66}$$

where z is still the cartesian vertical direction as seen on Fig. 11.

E Vorticity

In fluid mechanics one normally defines the vorticity as the curl of the fluid velocity: $\boldsymbol{\nabla} \times \mathbf{u}$. In the following we show that the parallel component of the vorticity of the $\mathbf{E} \times \mathbf{B}$-drift in our geometry is simply the perpendicular laplacian of the electrostatic potential over B. That is:

$$\Omega_{0,\parallel} = \left(\boldsymbol{\nabla} \times \mathbf{u}^E\right) \cdot \hat{\mathbf{B}} = \frac{\nabla_\perp^2 \phi}{B}. \tag{67}$$

We will start with deriving the parallel component without any assumptions of the geometry of the B-field:

$$\begin{aligned}
\left(\boldsymbol{\nabla} \times \mathbf{u}^E\right) \cdot \hat{\mathbf{B}} &= -\boldsymbol{\nabla} \times \left(\frac{\boldsymbol{\nabla}\phi \times \hat{\mathbf{B}}}{B}\right) \cdot \hat{\mathbf{B}} \\
&= \frac{1}{B}\Big(\boldsymbol{\nabla} \times \Big(\hat{\mathbf{B}} \times \boldsymbol{\nabla}\phi\Big)\Big) \cdot \hat{\mathbf{B}} + \left[\left(\boldsymbol{\nabla}\frac{1}{B}\right) \times \Big(\hat{\mathbf{B}} \times \boldsymbol{\nabla}\phi\Big)\right] \cdot \hat{\mathbf{B}} && \text{using (45k)} \\
&= \frac{1}{B}\Big[\boldsymbol{\nabla} \cdot \Big((\boldsymbol{\nabla}\phi)\hat{\mathbf{B}} - \hat{\mathbf{B}}(\boldsymbol{\nabla}\phi)\Big)\Big] \cdot \hat{\mathbf{B}} + \left[\left(\boldsymbol{\nabla}\frac{1}{B}\right) \times \Big(\hat{\mathbf{B}} \times \boldsymbol{\nabla}\phi\Big)\right] \cdot \hat{\mathbf{B}} && \text{using (45l)} \\
&= \frac{1}{B}\Big[(\boldsymbol{\nabla}\phi) \cdot \Big(\boldsymbol{\nabla}\hat{\mathbf{B}}\Big) + (\boldsymbol{\nabla} \cdot \boldsymbol{\nabla}\phi)\hat{\mathbf{B}} - \hat{\mathbf{B}} \cdot \boldsymbol{\nabla}\boldsymbol{\nabla}\phi - \Big(\boldsymbol{\nabla} \cdot \hat{\mathbf{B}}\Big)\boldsymbol{\nabla}\phi\Big] \cdot \hat{\mathbf{B}} \\
&\quad + \left[\left(\boldsymbol{\nabla}\frac{1}{B}\right) \times \Big(\hat{\mathbf{B}} \times \boldsymbol{\nabla}\phi\Big)\right] \cdot \hat{\mathbf{B}} && \text{using (45f)}
\end{aligned}$$

Now, from the dot product rule, Eq. (45g), we have that

$$\begin{aligned}
\boldsymbol{\nabla}\Big(\hat{\mathbf{B}} \cdot \boldsymbol{\nabla}\phi\Big) &= \boldsymbol{\nabla}\hat{\mathbf{B}} \cdot \boldsymbol{\nabla}\phi + \hat{\mathbf{B}} \cdot \boldsymbol{\nabla}\boldsymbol{\nabla}\phi \Leftrightarrow \\
-\hat{\mathbf{B}} \cdot \boldsymbol{\nabla}\boldsymbol{\nabla}\phi &= -\boldsymbol{\nabla}\Big(\hat{\mathbf{B}} \cdot \boldsymbol{\nabla}\phi\Big) + \Big(\boldsymbol{\nabla}\hat{\mathbf{B}}\Big) \cdot (\boldsymbol{\nabla}\phi)
\end{aligned}$$

Inserting this gives

$$\begin{aligned}
\left(\boldsymbol{\nabla} \times \mathbf{u}^E\right) \cdot \hat{\mathbf{B}} = \frac{1}{B}\Big[(\boldsymbol{\nabla}\phi) \cdot \Big(\boldsymbol{\nabla}\hat{\mathbf{B}}\Big) + (\boldsymbol{\nabla} \cdot \boldsymbol{\nabla}\phi)\hat{\mathbf{B}} - \boldsymbol{\nabla}\Big(\hat{\mathbf{B}} \cdot \boldsymbol{\nabla}\phi\Big) + \Big(\boldsymbol{\nabla}\hat{\mathbf{B}}\Big) \cdot (\boldsymbol{\nabla}\phi) - \Big(\boldsymbol{\nabla} \cdot \hat{\mathbf{B}}\Big)\boldsymbol{\nabla}\phi\Big] \cdot \hat{\mathbf{B}} \\
+ \left[\left(\boldsymbol{\nabla}\frac{1}{B}\right) \times \Big(\hat{\mathbf{B}} \times \boldsymbol{\nabla}\phi\Big)\right] \cdot \hat{\mathbf{B}}
\end{aligned}$$

Using the scaled vector product rule for the divergence, Eq. (45i) gives

$$\begin{aligned}
\boldsymbol{\nabla} \cdot \Big(\hat{\mathbf{B}}\hat{\mathbf{B}} \cdot \boldsymbol{\nabla}\phi\Big) &= \Big(\hat{\mathbf{B}} \cdot \boldsymbol{\nabla}\phi\Big)\Big(\boldsymbol{\nabla} \cdot \hat{\mathbf{B}}\Big) + \hat{\mathbf{B}} \cdot \boldsymbol{\nabla}\Big(\hat{\mathbf{B}} \cdot \boldsymbol{\nabla}\phi\Big) \Leftrightarrow \\
-\boldsymbol{\nabla}\Big(\hat{\mathbf{B}} \cdot \boldsymbol{\nabla}\phi\Big) \cdot \hat{\mathbf{B}} &= -\boldsymbol{\nabla} \cdot \Big(\hat{\mathbf{B}}\hat{\mathbf{B}} \cdot \boldsymbol{\nabla}\phi\Big) + \Big(\hat{\mathbf{B}} \cdot \boldsymbol{\nabla}\phi\Big)\Big(\boldsymbol{\nabla} \cdot \hat{\mathbf{B}}\Big).
\end{aligned}$$

Inserting this gives

$$\begin{aligned}
\left(\boldsymbol{\nabla} \times \mathbf{u}^E\right) \cdot \hat{\mathbf{B}} = \frac{1}{B}\Big[\boldsymbol{\nabla} \cdot \Big(\Big[\boldsymbol{\nabla} - \hat{\mathbf{B}}\hat{\mathbf{B}} \cdot \boldsymbol{\nabla}\Big]\phi\Big) + \Big(\hat{\mathbf{B}} \cdot \boldsymbol{\nabla}\phi\Big)\Big(\boldsymbol{\nabla} \cdot \hat{\mathbf{B}}\Big)\Big] \\
+ \frac{1}{B}\Big[(\boldsymbol{\nabla}\phi) \cdot \Big(\boldsymbol{\nabla}\hat{\mathbf{B}}\Big) + \Big(\boldsymbol{\nabla}\hat{\mathbf{B}}\Big) \cdot (\boldsymbol{\nabla}\phi) - \Big(\boldsymbol{\nabla} \cdot \hat{\mathbf{B}}\Big)\boldsymbol{\nabla}\phi\Big] \cdot \hat{\mathbf{B}} \\
+ \left[\left(\boldsymbol{\nabla}\frac{1}{B}\right) \times \Big(\hat{\mathbf{B}} \times \boldsymbol{\nabla}\phi\Big)\right] \cdot \hat{\mathbf{B}}
\end{aligned} \tag{70}$$

E.1 Parallel Vorticity in our Geometry

We quickly reiterate the results, Eqs. (57), (60), (64) specific to the geometry of our B-field:

$$\mathbf{B} = \frac{B_0 R_0}{R}\hat{\boldsymbol{\zeta}}, \qquad \boldsymbol{\nabla}\hat{\mathbf{B}} = -\frac{1}{R}\hat{\boldsymbol{\zeta}}\hat{\mathbf{R}}, \qquad \boldsymbol{\nabla}\left(\frac{1}{B}\right) = \frac{1}{B_0 R_0}\hat{\mathbf{R}}.$$

The terms with the divergence of $\hat{\mathbf{B}}$ vanishes due to the "no magnetic monopole" Maxwell equation:

$$\boldsymbol{\nabla}\cdot\hat{\mathbf{B}} = \boldsymbol{\nabla}\cdot\left(\frac{\mathbf{B}}{B}\right) = \frac{1}{B}\boldsymbol{\nabla}\cdot\mathbf{B} + \mathbf{B}\cdot\left(\boldsymbol{\nabla}\frac{1}{B}\right) = \frac{B}{B_0 R_0}\hat{\mathbf{B}}\cdot\hat{\mathbf{R}} = 0.$$

Meanwhile the last term of Eq. (70) gives:

$$\left[\left(\boldsymbol{\nabla}\frac{1}{B}\right)\times\left(\hat{\mathbf{B}}\times\boldsymbol{\nabla}\phi\right)\right]\cdot\hat{\mathbf{B}} = \frac{\hat{\mathbf{B}}}{B_0 R_0}\cdot\left(\hat{\mathbf{R}}\times\left(\hat{\mathbf{B}}\times\boldsymbol{\nabla}\phi\right)\right) \tag{71a}$$

$$= \frac{\hat{\mathbf{B}}\times\boldsymbol{\nabla}\phi}{B_0 R_0}\cdot\left(\hat{\mathbf{B}}\times\hat{\mathbf{R}}\right) = -\frac{\hat{\mathbf{z}}\cdot\left(\hat{\mathbf{B}}\times\boldsymbol{\nabla}\phi\right)}{B_0 R_0} = -\frac{\boldsymbol{\nabla}\phi\cdot\left(\hat{\mathbf{z}}\times\hat{\mathbf{B}}\right)}{B_0 R_0} = \frac{\partial_R\phi}{B_0 R_0}. \tag{71b}$$

Finally the terms with $\boldsymbol{\nabla}\hat{\mathbf{B}}$ gives:

$$\frac{(\boldsymbol{\nabla}\phi)\cdot\left(\boldsymbol{\nabla}\hat{\mathbf{B}}\right)}{B}\cdot\hat{\mathbf{B}} = -\frac{(\boldsymbol{\nabla}\phi)\cdot\hat{\boldsymbol{\zeta}}\hat{\mathbf{R}}}{B_0 R_0}\cdot\hat{\mathbf{B}} = -\frac{\partial_\parallel\phi}{B_0 R_0}\left(\hat{\mathbf{R}}\cdot\hat{\mathbf{B}}\right) = 0 \tag{72a}$$

$$\frac{\left(\boldsymbol{\nabla}\hat{\mathbf{B}}\right)\cdot(\boldsymbol{\nabla}\phi)}{B}\cdot\hat{\mathbf{B}} = -\frac{\hat{\boldsymbol{\zeta}}\hat{\mathbf{R}}\cdot(\boldsymbol{\nabla}\phi)}{B_0 R_0}\cdot\hat{\mathbf{B}} = -\frac{\partial_R\phi}{B_0 R_0}. \tag{72b}$$

We see that (72b) cancels (71b). Thus, almost all terms of Eq. (70) cancels and we are only left with:

$$\left(\boldsymbol{\nabla}\times\mathbf{u}^E\right)\cdot\hat{\mathbf{B}} = \frac{\nabla_\perp^2\phi}{B}, \tag{73}$$

where the perpendicular laplacian is defined as:

$$\nabla_\perp^2 \equiv \boldsymbol{\nabla}\cdot\left(\boldsymbol{\nabla}-\boldsymbol{\nabla}_\parallel\right) = \boldsymbol{\nabla}\cdot\left(\boldsymbol{\nabla}-\hat{\mathbf{B}}\hat{\mathbf{B}}\cdot\boldsymbol{\nabla}\right). \tag{74}$$

F Collisional Friction

In the following we derive the diffusion terms of the density equation originating from elastic collisions in the plasma. We only consider first ionisation and assume quasineutrality: $n_i \approx n_e \equiv n$. We can use the zeroth order drifts and the result from Braginskii, [4, Eq. (2.6), (2.9)] to estimate the total collisional friction force between ions and electrons by:

$$\begin{aligned}
\mathbf{f}_{ie}^R &= \mathbf{f}_{ie,T}^R + \mathbf{f}_{ie,u}^R, \quad \text{where} \\
\mathbf{f}_{ie,T}^R &= -0.71 n_e \boldsymbol{\nabla} T_e - \frac{3}{2}\frac{n_e\nu_{ei}}{\omega_{ce}}\hat{\mathbf{B}}\times\boldsymbol{\nabla}T_e \\
\mathbf{f}_{ie,u}^R &= -m_e n_e \nu_{ei}\big(0.51(\mathbf{u}_{e,\parallel}-\mathbf{u}_{i,\parallel}) + (\mathbf{u}_{e,\perp}-\mathbf{u}_{i,\perp})\big) \\
&\approx -m_e n_e \nu_{ei}\big(0.51(\mathbf{u}_{e,\parallel}-\mathbf{u}_{i,\parallel}) + \left(\mathbf{u}_\perp^E-\mathbf{u}_\perp^E\right) + \left(\mathbf{u}_{e,\perp}^d-\mathbf{u}_{i,\perp}^d\right) + \left(\mathbf{u}_{e,\perp}^{\mathrm{cf}}-\mathbf{u}_{i,\perp}^{\mathrm{cf}}\right)\big) \\
&= -m_e n_e \nu_{ei}\left(0.51(\mathbf{u}_{e,\parallel}-\mathbf{u}_{i,\parallel}) + \frac{\boldsymbol{\nabla}_\perp(p_e+p_i)\times\hat{\mathbf{B}}}{enB} - \frac{m_e u_{e,\parallel}^2 + m_i u_{i,\parallel}^2}{eB_0 R_0}\hat{\mathbf{R}}\times\hat{\mathbf{B}}\right).
\end{aligned}$$

Here, ν_{ei} is the collision frequency of electron-ion collisions which is given analytically by [10, Eq. (11.22)]:

$$\nu_{ei} = \frac{2^{1/2} n_i Z^2 e^4 \ln\Lambda}{12\pi^{3/2} e_0^2 m_e^{1/2} T_e^{3/2}}, \quad \text{where} \quad \ln\Lambda = \ln\left(\frac{12\pi n\lambda_D^3}{Z}\right), \qquad \lambda_D = \sqrt{\frac{\varepsilon_0 T_e}{n_e e^2}}.$$

We will assume the temperature to be slowly varying ($\boldsymbol{\nabla} T_e \approx \mathbf{0}$), such that we can neglect the thermal collisional friction: $\mathbf{f}^R_{ie,T} \approx \mathbf{0}$.

By assuming the neutrals to be much slower than the electrons, we can estimate the collisional friction force between neutral atoms and charges [12, p. 23]:

$$\begin{aligned}\mathbf{f}^R_{a\sigma} &= -m_\sigma n_\sigma \nu_{\sigma a}(\mathbf{u}_\sigma - \mathbf{u}_n) \\ &\approx -m_\sigma n_\sigma \nu_{\sigma a}\big(\mathbf{u}_{\sigma,\parallel} + \mathbf{u}^E_\perp + \mathbf{u}^d_{\sigma,\perp} + \mathbf{u}^{\mathrm{cf}}_{\sigma,\perp}\big) \\ &= -m_\sigma n_\sigma \nu_{\sigma a}\left(\mathbf{u}_{\sigma,\parallel} - \frac{\boldsymbol{\nabla}_\perp \phi \times \hat{\mathbf{B}}}{B} - \frac{\boldsymbol{\nabla}_\perp p_\sigma \times \hat{\mathbf{B}}}{n_\sigma q_\sigma B} + \frac{m_\sigma u^2_{\sigma,\parallel}}{q_\sigma B_0 R_0}\hat{\mathbf{R}} \times \hat{\mathbf{B}}\right).\end{aligned}$$

Here $\nu_{\sigma a}$ is the frequency of collisions between charge σ and atom a which is given by [12, p. 169]:

$$\nu_{\sigma a} = \frac{8\sqrt{2}}{3\sqrt{\pi}} n_a \sqrt{\frac{T_e}{m_e}}\sigma_{ea}. \tag{75}$$

Note, σ_{ea} is the elastic collision cross section between the electron and neutral atoms in the plasma. According to [11], the cross section has a value of $6 \times 10^{-21}\,\mathrm{m}^2$ at an electron temperature of $T_e = T_{e0} = 10\,\mathrm{eV}$. These friction forces gives the collisional friction drift from Eq. (35b):

$$\mathbf{u}^R_{\sigma,\perp} = \mathbf{u}^R_{\sigma'\sigma,\perp} + \mathbf{u}^R_{a\sigma,\perp}, \quad \text{where} \tag{76a}$$

$$\mathbf{u}^R_{\sigma'\sigma,\perp} = \frac{n_e \nu_{ei}}{n_\sigma \omega_{ce}}\left(\frac{\boldsymbol{\nabla}_\perp (p_e + p_i)}{enB} + \frac{m_e u^2_{e,\parallel} + m_i u^2_{i,\parallel}}{eB_0 R_0}\hat{\mathbf{R}}\right), \quad \text{and} \tag{76b}$$

$$\mathbf{u}^R_{a\sigma,\perp} = -\frac{m_\sigma \nu_{\sigma a}}{q_\sigma B}\left(\frac{\boldsymbol{\nabla}_\perp \phi}{B} + \frac{\boldsymbol{\nabla}_\perp p_\sigma}{q_\sigma n_\sigma B} - \frac{m_\sigma u^2_{\sigma,\parallel}}{q_\sigma B_0 R_0}\hat{\mathbf{R}}\right). \tag{76c}$$

The latter drift is the Pedersen drift (with a centrifugal force).

F.1 Electron Density Diffusion

Due to the symmetry of the NORTH machine, which is the subject of this study, we assume the parallel fluid velocity to be 0, $u_{\sigma,\parallel} \approx 0$. Furthermore we neglect temperature variations, $\boldsymbol{\nabla} T_\sigma$, and assume quasineutrality, Eq. (24).

F.1.1 Diffusion from electron-ion collisions

With the approximations, the drift from electron-ion collisionsm in Eq. (76b) simplifies to:

$$\begin{aligned}\mathbf{u}^R_{ie,\perp} &\approx -\frac{m_e \nu_{ei}\boldsymbol{\nabla}_\perp (p_e + p_i)}{n(eB)^2} = -\nu_{ei}\rho^2_{Le}\frac{\boldsymbol{\nabla}_\perp (p_e + p_i)}{nT_e} \\ &= -\nu_{ei}\rho^2_{Le}\left(\frac{\boldsymbol{\nabla}_\perp (T_e + T_i)}{T_e} + \frac{1}{n}\left(1 + \frac{T_i}{T_e}\right)\boldsymbol{\nabla}_\perp n\right) \\ &\approx -\frac{\nu_{ei}\rho^2_{Le}}{n}\left(1 + \frac{T_i}{T_e}\right)\boldsymbol{\nabla}_\perp n',\end{aligned}$$

where ρ_{Le} is the electron Larmor radius:

$$\rho^2_{L,e} = \frac{m_e T_e}{e^2 B^2}.$$

The resulting drift gives rise to the classical diffusion term when taking the divergence of the flux:

$$-\boldsymbol{\nabla}\cdot\left(n\mathbf{u}^R_{ie,\perp}\right) = \boldsymbol{\nabla}\cdot\left(D_{ei}\left(1 + \frac{T_i}{T_e}\right)\boldsymbol{\nabla}_\perp n\right), \tag{77}$$

where the classical diffusion coefficient in our model is determined from the characteristic scales of the system (n_0, T_{e0}, B_0):

$$D_{ei} \equiv \nu_{ei0}\,\rho^2_{Le0} \equiv k_{ei}\,n\,\rho^2_{Le0}, \tag{78a}$$

$$\rho^2_{Le0} \equiv \frac{m_e T_{e0}}{e^2 B_0^2} \quad k_{ei} \equiv \frac{2^{1/2} Z^2 e^4 \ln\Lambda_0}{12\pi^{3/2} e_0^2 m_e^{1/2} T_{e0}^{3/2}}, \quad \ln\Lambda_0 \equiv \ln\left(\frac{12\pi n_0 \lambda^3_{D0}}{Z}\right), \quad \lambda_{D0} \equiv \sqrt{\frac{\varepsilon_0 T_{e0}}{n_0 e^2}}. \tag{78b}$$

F.1.2 Diffusion from neutral-electron collisions

With the same approximations as for the electron-ion collisions above, we can simplify the Pedersen drift, Eq. (76c) originating from collisions between neutral atoms and charges:

$$\mathbf{u}^R_{ae,\perp} \approx \frac{m_e \nu_{ea}}{eB}\left(\frac{\boldsymbol{\nabla}_\perp \phi}{B} - \frac{\boldsymbol{\nabla}_\perp p_\sigma}{enB}\right) = \nu_{en}\rho^2_{Le}\left(\frac{e}{T_e}\boldsymbol{\nabla}_\perp \phi - \frac{\boldsymbol{\nabla}_\perp p_e}{nT_e}\right)$$
$$= \nu_{en}\rho^2_{Le}\left(\frac{e}{T_e}\boldsymbol{\nabla}_\perp \phi - \left(\frac{\boldsymbol{\nabla}_\perp T_e}{T_e} + \frac{\boldsymbol{\nabla}_\perp n}{n}\right)\right) \approx \nu_{en}\rho^2_{Le}\left(\frac{e}{T_e}\boldsymbol{\nabla}_\perp \phi - \frac{\boldsymbol{\nabla}_\perp n}{n}\right).$$

Now, according to [10, Eq. (12.23)], the perpendicular E-field can be approximated by:

$$\boldsymbol{\nabla}_\perp \phi \approx \frac{T_i}{ne}\boldsymbol{\nabla}_\perp n.$$

With this the divergence of the Pedersen flux also turns into a diffusion term:

$$-\boldsymbol{\nabla}\cdot\left(n\mathbf{u}^R_{ae,\perp}\right)) \approx \boldsymbol{\nabla}\cdot\left(D_{ea}\left(1+\frac{T_i}{T_e}\right)\boldsymbol{\nabla}_\perp n\right), \tag{79}$$

where the diffusion coefficient is approximated by:

$$D_{ea} \equiv \nu_{ea0}\,\rho^2_{Le0}. \tag{80a}$$

$$\rho^2_{Le0} \equiv \frac{m_e T_{e0}}{e^2 B_0^2} \quad \nu_{ea0} = \frac{8\sqrt{2}}{3\sqrt{\pi}} n_{a0}\sqrt{\frac{T_{e0}}{m_e}}\sigma_{ea}, \quad n_{a0} = 1.2\cdot 10^{19}\,\mathrm{m}^{-3}, \quad \sigma_{ea} = 6\times 10^{-21}\,\mathrm{m}^2. \tag{80b}$$

Here the density of neutral atoms n_{a0} was estimated from the typical He gas pressure in NORTH which is on the order of $5\cdot 10^{-4}$ mbar corresponding to a particle density of $\sim 1.2\cdot 10^{19}\,\mathrm{m}^{-3}$.

G Implementation

This section includes further details on the implementation setup.

G.1 High-Performing Computing setup

All simulations were executed at the high-performance computing (HPC) cluster called Niflheim, which is located at the Technical University of Denmark. The GitHub documentation [1] explains in detail how to run the simulations and data analysis on this specific environment, while the documentation for the Bout++ framework have specific guides on running simulations on other similar HPC-environments [2].

G.2 Coordinates in Bout++

Bout++ by default works in Clebsh coordinates where [2]

$$\mathbf{B}_{\text{Clebsch}} = \mathbf{e}^3 \times \mathbf{e}^1 = \frac{1}{J}\mathbf{e}_2,$$

with the definitions of the basis vectors introduced in Section B. The magnetic field in Bout++ is therefore aligned with the second covariant basis-vector. The coordinates in Bout are called (X, Y, Z), so the following mapping needs to be done:

Parameter	Toroidal Coordinate	Bout
u^1	r	X
u^2	ζ	Y
u^3	θ	Z

We reserve capital (X, Y, Z) for the bout-coordinates, which are not to be confused with the cartesian coordinates (x, y, z) from (52). Note, that in Bout++ the coordinates are normalised such that $X \in [0, 1]$, $Y \in [0, 2\pi]$, $Z \in [0, 2\pi]$, why we must have:

$$X = \frac{\rho_s}{a} r', \qquad Y = \zeta = \zeta', \qquad Z = \theta = \theta'.$$

We distinguish between $\mathbf{B}$ (the usual field in toroidal coordinates) and $\mathbf{B}_{\text{Clebsch}}$. The two fields can be related to each other through:

$$\mathbf{B} = B\,\mathbf{e}_2 = B\,J\,\mathbf{B}_{\text{Clebsch}}. \tag{81}$$

The norm of the Clebsch-B-field is

$$B_{\text{Clebsch}} = \sqrt{\mathbf{B}_{\text{Clebsch}} \cdot \mathbf{B}_{\text{Clebsch}}} \tag{82a}$$

$$= \frac{\sqrt{\mathbf{e}_2 \cdot \mathbf{e}_2}}{J} \tag{82b}$$

$$= \frac{\sqrt{g_{22}}}{J}. \tag{82c}$$

G.3 Metric coefficients and Jacobian in Bout

Bout++ supports providing metric coefficients and Jacobian as input. The Jacobian (51) is 0 at the center of the torus $r = 0$ as it should be. However, this is a problem in Bout++, which requires the Jacobian to be strictly positive in the entire range $X \in [0, 1]$ (even if the first inner point $X_{\text{start}} > 0$ as in our case). Since the lowest possible r-value is $\frac{\Delta r}{2}$, we can circumvent the problem without loosing accuracy by defining the following Jacobian in Bout:

$$J_{\text{Bout}} = \max\left(r, \frac{\Delta r}{2}\right)\left(R_0 + \max\left(r, \frac{\Delta r}{2}\right)\cos\theta\right)$$

The same trick was used for defining the metric coefficients g_{22}, g_{33} from Eq. (50).

G.4 Simulation mesh

We used the default mesh generator in Bout++, where one simply gives the number of points in each direction. Note that this results in gridpoints lying much closer together at the center $X \approx 0$ compared to at the boundary $X = 1$. Table 1 presents an overview of the mesh parameters used.

Input	Value	Description
`mxg`	2	No. of ghost points for X-axis
`myg`	0	No. of ghost points for Y-axis (B-field direction)
`NX`	84	No. of inner points and ghost points along X-axis
`NY`	0	No. of inner points along Y-axis (B-field direction)
`NZ`	256	No. of inner points along Z-axis

Table 1: Overview of parameters used to generate the simulation mesh.

G.5 Implementation of BCs and Center Singularity

The Neumann BCs at $r = a$ were applied using `neumann_o2` which sets the BC halfway between the ghost cell and grid cell at a 2nd order accuracy.

At the center of the torus, $r = 0$, there is a problem, since there is an artificial boundary with ghost points, but no guarantee that the fields will be well-defined across the boundary. To deal with this, we used the method from [12, Ch. 9] which is illustrated in Figure 12 for the case of two

ghost points. The boundary $r = 0$ is placed halfway between the last ghost point and first r-point. Assuming the r-axis is divided in intervals of Δr, the first r-value is $\frac{\Delta r}{2}$. For any field $f(r, \theta)$ we then require

$$f\left(\frac{\Delta r}{2}, \theta_0\right) = f\left(-\frac{\Delta r}{2}, (\theta_0 + \pi) \bmod 2\pi\right)$$
$$f\left(\frac{3\Delta r}{2}, \theta_0\right) = f\left(-\frac{3\Delta r}{2}, (\theta_0 + \pi) \bmod 2\pi\right),$$

and one can continue the system for more ghost points. The practical implementation almost followed one-to-one the code by Løiten in [12] and is seen on GitHub [1] in the class with header file `toroidalBCs.hxx`.

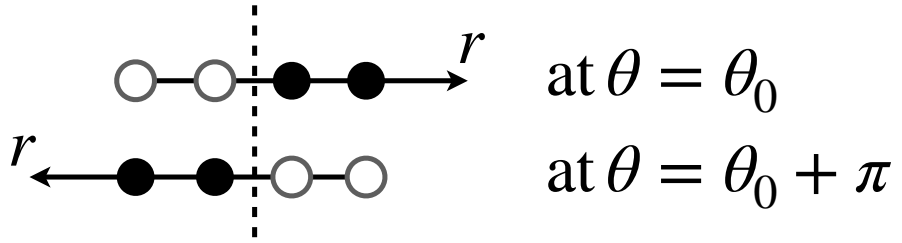

Figure 12: Illustration of how ghosts points are matched across the boundary $r = 0$ at the center of the torus. Outlined points represent ghost points, whereas filled points are the inner points.

G.6 Curvature operator

To calculate the curvature operator $\mathcal{C}(f)$ from Eq. (66) in Bout++, we need to translate the vertical derivative ∂_z from cartesian to curvilinear coordinates using the chain rule:

$$\frac{\partial}{\partial z} = \frac{\partial r}{\partial z}\frac{\partial}{\partial r} + \frac{\partial \theta}{\partial z}\frac{\partial}{\partial \theta} + \frac{\partial \zeta}{\partial z}\frac{\partial}{\partial \zeta} \tag{83}$$
$$= \frac{z}{\sqrt{x^2 + z^2}}\frac{\partial}{\partial r} + \frac{x}{x^2 + z^2}\frac{\partial}{\partial \theta} \tag{84}$$
$$= \sin\theta\,\frac{\partial}{\partial r} + \frac{\cos\theta}{r}\,\frac{\partial}{\partial \theta} \tag{85}$$

In normalised coordinates for the ESEL-implementation in Bout++ the curvature operator then becomes:

$$\mathcal{C}' = \frac{2\rho_{s,0}^2}{aR_0}\left(\sin Z\,\frac{\partial}{\partial X} + \frac{\cos Z}{X}\,\frac{\partial}{\partial Z}\right). \tag{86}$$

G.7 Advective Derivative and Poisson bracket

To lowest order when only accounting for the $\mathbf{E} \times \mathbf{B}$ drift, the comoving derivative is

$$\frac{\mathrm{d}}{\mathrm{d}t} = \frac{\partial}{\partial t} + \mathbf{v}_E \cdot \boldsymbol{\nabla} = \frac{\partial}{\partial t} - \frac{\boldsymbol{\nabla}\phi \times \mathbf{b}}{B} \cdot \boldsymbol{\nabla}. \tag{87}$$

In [12, A. I] it is shown that the advective part of the derivative in Clebsch-coordinates is

$$\mathbf{v}_{E,\mathrm{Clebsch}} \cdot \boldsymbol{\nabla} = -\frac{\boldsymbol{\nabla}\phi \times \mathbf{b}}{B_{\mathrm{Clebsch}}} \cdot \boldsymbol{\nabla} \tag{88a}$$
$$= \frac{1}{g_{22}}\Big(g_{21}\{\phi, \cdot\}_{2,1} + g_{22}\{\phi, \cdot\}_{3,1} + g_{23}\{\phi, \cdot\}_{1,2}\Big), \tag{88b}$$

where we recall the definition of the Poisson bracket:

$$\{f, g\}_{ij} = \left(\frac{\partial}{\partial u^i} f\right)\frac{\partial}{\partial u^j} g - \left(\frac{\partial}{\partial u^j} f\right)\frac{\partial}{\partial u^i} g. \tag{89}$$

For an orthogonal coordinate system such as ours, the metric tensor is diagonal (as seen in (50)) and (88) reduces to:

$$\mathbf{v}_{E,\text{Clebsch}} \cdot \boldsymbol{\nabla} = \{\phi, \cdot\}_{3,1}. \tag{90}$$

From the Clebsch-form we obtain the advective term in our toroidal coordinate system:

$$\begin{aligned}
\mathbf{v}_E \cdot \boldsymbol{\nabla} &= -\frac{\boldsymbol{\nabla}\phi \times \mathbf{b}}{B} \cdot \boldsymbol{\nabla} \\
&= \frac{B_{\text{Clebsch}}}{B} \mathbf{v}_{E,\text{Clebsch}} \cdot \boldsymbol{\nabla} \\
&= \frac{\sqrt{g_{22}}}{JB} \{\phi, \cdot\}_{3,1} \\
&= \frac{(R_0 + r\cos\theta)}{r(R_0 + r\cos\theta)B} \{\phi, \cdot\}_{\theta,r} \\
&= \frac{(R_0 + r\cos\theta)}{rB_0R_0} \{\phi, \cdot\}_{\theta,r} \\
&= \frac{1}{B_0}\left(\frac{1}{r} + \frac{\cos\theta}{R_0}\right) \{\phi, \cdot\}_{\theta,r}.
\end{aligned}$$

The non-dimensionalized advective operator then is

$$\mathbf{v}'_{E'} \cdot \boldsymbol{\nabla}' = \left(\frac{1}{r'} + \frac{\rho_s \cos\theta}{R_0}\right) \{\phi, \cdot\}_{\theta,r'} \tag{92}$$

In Bout-coordinates this is:

$$\mathbf{v}'_{E'} \cdot \boldsymbol{\nabla}' = \left(\frac{\rho_s}{aX} + \frac{\rho_s \cos Z}{R_0}\right) \{\phi, \cdot\}_{Z,X}$$

G.8 Probes

In order to see fast fluctuations in the density and temperature without handling extensive amounts of data (which would also slow down the simulation), a series of local probes are programmed in the domain. The density and temperature is sampled at the probe positions with a frequency that is > 1000 times faster than the data dumps for the entire domain. In total 10 probes are used in a line with $\theta = 0$, and their radial positions are summarized in [13].

References

[1] Asbjørn Clod Pedersen and Rune Højlund. *GitHub Repository: North Simulation*. https://github.com/PPFE-Turbulence/north-simulation. 2022.

[2] Ben Dudson. *Bout++ Documentation*. June 2022. URL: `https://bout-dev.readthedocs.io/en/latest/user_docs/advanced_install.html`.

[3] S. I Braginsdkii. *Transport Processes in a Plasma*. 1965.

[4] S. I. Braginskii. *Transport processes in a plasma*. Ed. by Acad. M. A. Leontovich. Vol. 1. Consultants Bureau, 1965, pp. 205–311.

[5] B. D. Dudson et al. "BOUT++: A framework for parallel plasma fluid simulations". In: *Computer Physics Communications* 180.9 (Sept. 2009), pp. 1467–1480. ISSN: 00104655. DOI: `10.1016/j.cpc.2009.03.008`.

[6] B. D. Dudson et al. "BOUT++: Recent and current developments". In: *Journal of Plasma Physics* 81.1 (Jan. 2015). ISSN: 14697807. DOI: `10.1017/S0022377814000816`.

[7] O. E. Garcia et al. "Turbulence and intermittent transport at the boundary of magnetized plasmas". In: *Physics of Plasmas* 12.6 (2005), pp. 1–14. ISSN: 1070664X. DOI: `10.1063/1.1925617`.

[8] O. E. Garcia et al. "Turbulence simulations of blob formation and radial propagation in toroidally magnetized plasmas". In: *Physica Scripta T* T122 (2006), pp. 89–103. ISSN: 02811847. DOI: 10.1088/0031-8949/2006/T122/013.

[9] R Glowinski et al. *Flux Coordinates and Magnetic Field Structure*. Springer-Verlag, 1991. ISBN: 9783642755972.

[10] Robert Goldston and Paul Rutherford. *Introduction to Plasma Physics*. 1995. ISBN: 0750303255. DOI: 10.1201/9781439822074.

[11] Dmitry Levko. "Initial stage of beam-generated plasma with evaporating electrode". In: *Physics of Plasmas* 27 (2 2020). ISSN: 10897674. DOI: 10.1063/1.5126709.

[12] Michael Løiten. "Global numerical modeling of magnetized plasma in a linear device". Technical University of Denmark, 2017.

[13] Asbjørn Clod Pedersen and Rune Højlund. *"Reduced Fluid Simulations of Perpendicular Blob Propagation in the NORTH Tokamak". Project report from 2022*. 2022.

[14] Alexander Simon Thrysøe. "Influence of neutral particles on edge dynamics of magnetically confined plasmas". Technical University of Denmark, 2018.

[15] Alexander Simon Thrysøe. "Influence of neutral particles on edge dynamics of magnetically confined plasmas". In: (2018).